CFD Letters

Journal homepage:
https://semarakilmu.com.my/journals/index.php/CFD_Letters/index
ISSN: 2180-1363

Influence Evaluation of Open Propellers with Boss Cap Fins: Case Studies on Types B4-70 and Ka4-70

Berlian Arswendo Adietya[1], Husein Syahab[2], Mahendra Indiaryanto[3], Wasis Dwi Aryawan[4], I Ketut Aria Pria Utama[4,*]

[1] Department of Naval Architecture, Universitas Dipenogoro, Semarang, 50275, Indonesia
[2] Department of Naval Architecture, Institut Teknologi Kalimantan, Balikpapan, 76127, Indonesia
[3] National Research and Innovation Agency (BRIN), Indonesia
[4] Department of Naval Architecture, Institut Teknologi Sepuluh Nopember,Surabaya, 60111, Indonesia

ARTICLE INFO

Article history:
Received 29 August 2023
Received in revised form 21 September 2023
Accepted 22 October 2023
Available online 30 April 2024

Keywords:
B4-70; Energy Efficiency; Ka4-70; PBCF; Turbulence Modelling

ABSTRACT

Numerical analysis of fins effect on propeller performance was conducted, specifically using the B4-70 and Ka4-70 propellers. The study investigated different types of fins, including bare fins and PBCF (Propeller Boss Cap Fins) using computational fluid dynamics (CFD) simulations. The explicit algebraic stress model (EASM) based on Reynolds-Averaged Navier-Stokes (RANS) equations and turbulence modeling was employed to determine the optimal results. The main objective of this research was to enhance energy efficiency in ships by examining various open propeller configurations. The CFD simulation results for open propellers B4-70 and Ka4-70, with the addition of boss cap fins, revealed interesting phenomena. When the open propellers B4-70 and Ka4-70 were equipped with PBCF, they would experience an increase in efficiency (η0). This was because the performance of the fins functioned optimally when the advance ratio (J) is high, as evident from the high velocity values. Thus, with higher velocity and lower pressure in the boss cap region at high J values, there was an elevation in thrust force due to the reduction of hub vortex. In the case of open propeller B4-70 with added PBCF, there was an increase in the efficiency value (η0) ranging from 3% to 5% when J varied from 0 to 0.7. Similarly, for propeller Ka4-70 with the addition of PBCF, there was an increase in the efficiency value (η0) ranging from 1% to 3% when J varied from 0 to 0.7. Notably, the use of an Energy-Saving Device (ESD) in the form of PBCF can increase the efficiency of ship propeller, as reported in this paper. Consequently, these findings affirmed the reliability of the overall calculations using the CFD approach.

1. Introduction

The desire for energy saving and emission reduction is necessary in the marine industry. However, the energy saving devices (ESDs) are highly focused on ocean-going vessels for transportation. Maritime transportation is essential to international trade and the global economy. Sea

* *Corresponding author.*
E-mail address: kutama@na.its.ac.id (I Ketut Aria Pria Utama)

https://doi.org/10.37934/cfdl.16.9.143177

transportation is recognized as an effective energy-efficiencies mode of transportation compared to other modes based on the fuel consumption ratio per goods moved. The global economy's dependence on the shipping sector must be paid for by CO_2 emissions that are detrimental to the environment. In 2018, shipping activities produced 1056 million tons of CO_2 emissions, or around 2.89% of anthropogenic CO_2 emissions [1]. Japan and Canada have the same goal of a 40-45% reduction, while the European Union (EU) will reduce emissions by 55% in 2030 compared to 1990 and become neutral by 2050 [2]. Several offered solutions to reduce Greenhouse gas (GHG) emissions are recommended by International Maritime Organization (IMO), including improving the ship's efficiency, optimizing the ship's operation, and converting to alternative fuels [3]. Moreover, in Fourth IMO GHG Study 2020 [4] several alternative ship efficiencies currently available for the shipping industry. As the primary energy-efficiencies, Energy Saving Device (ESD) is one of the alternative energy-efficiencies. One of the most popular ESD are Propeller Boss Cap Fins (PBCF). They consist of a series of fins (which number is generally equal to the number of the propeller blades) attached at the boss cap of the hub with a negligible angle of attack. Their installation, by simply replacing the hub cap, is cheaper and the simplest. Exactly as their name imply, PBCFs act as post-swirl appendages that, by reducing the hub vortex, increase the propeller efficiency. The reduction of the hub vortex (i.e., the drag associated to the suction pressure acting on the hub), however, is not the only way PBCF acts to improve efficiency. Also delivering a negative torque to the propeller axis or positively influencing the thrust delivered by the blades at constant absorbed torque are ways through which PBCF allows energy saving. Preliminary research on PBCF that is computational fluid dynamic (CFD) calculations of model scale efficiency of PBCF applied to different propellers [5] , also analyses of the influence of design parameters variations for PBCF on hub vortex reduction by [6] showed efficiency improvements no higher than 2% depending on the loading configuration of the PBCF itself, CFD Analysis into the Effect of using Propeller Boss Cap Fins (PBCF) on open water test, Case Study with Propeller B-Series and Kaplan-Series [7].

Utilizing an Electrostatic Discharge (ESD) system within the framework of open propeller has the potential to augment propeller thrust, whereas the incorporation of a Propeller Boss Cap Fins (PBCF) can enhance propeller efficiency. These improvements hold significant advantages for the operation of commercial vessels and traditional fishing boats, particularly during fishing endeavors. This is due to their indirect contribution to the vessel's functions, influenced by the dynamics of fishing gear [8], as well as for catamaran-style fishing vessels [9]. The application of these technologies is also viable for submarines, where the specialized criteria of generating substantial thrust in a noiseless manner are paramount [10]. Similarly, the benefits extend to niche applications like glass-bottom tourism boats [11]. Numerous studies examining duct systems, including the impact of a Pre-Duct on Ship Propeller-Hull dynamics, have expounded on the tendency of a pre-duct addition to enhance hull efficiency. However, this enhancement may come at the cost of reduced propeller efficiency in open water settings [12]. These investigations underline the need for a comprehensive approach when engineering propulsion systems for various aquatic applications.

However, implementing these solutions may be challenging for retrofitting purposes, as they involve significant modifications to the hull, rudder, or the addition of stator fins [13-16]. Instead, an alternative ESD can be considered, which allows for compliance with the Energy Efficiency Operation Index (EEOI) requirements without extensive modifications. Among the ESD components, PBCF is widely used. PBCF consists of fins attached to the hub boss cap at a small angle of attack, typically matching the number of propeller blades. The installation of PBCF is cost-effective and straightforward, requiring only the replacement of the hubcap. Previous CFD research has shown that open propellers, particularly the B-Series, perform well with PBCF [7]. In this study, CFD analysis was conducted to assess the hydrodynamic performance of propellers, considering turbulent

parameters [16] and the influence of flow rate [17]. The investigation focused on combining PBCF propeller types after studying the performance of open propellers (B-Series and Kaplan). Numerical simulations incorporated flow field distributions to analyze the impact of PBCF configurations on propulsion hydrodynamics.

To improve the prediction accuracy compared to the linear eddy-viscosity model and address limitations in turbulence modeling, the explicit algebraic stress model (EASM) was utilized. Unlike most turbulence models in the past, EASM aims to provide better predictions rather than avoiding singularities in turbulence modelling [18]. In this two-equation turbulence model, the Reynolds stress was obtained by transforming the differential form of the turbulent model equations into an explicit algebraic expression. The model was further enhanced by incorporating an explicit nonlinear Reynolds stress term. EASM utilizes the eddy viscosity assumption and offers various advantages, including numerical efficiency compared to the algebraic Reynolds stress model (ARSM), better handling of the limitations of the linear eddy-viscosity model, capturing the anisotropy effect of Reynolds stress, avoiding numerical singularity, and improving model stability and CPU usage compared to the Reynolds Stress Turbulence Model (RSTM) [19]. On the other hand, EASM model outperforms the k–omega SST model in predicting viscous resistance. Nevertheless, the EASM model slightly underestimates viscous resistance by around 4% without energy-saving devices and 3% with such devices. Additionally, the calculated strength of the longitudinal vorticity is slightly lower compared to the observed vorticity [20].

This research involves conducting numerical analysis of open propellers equipped with PBCF. The case studies specifically focus on the B4-70 and Ka4-70 propellers. The novelty of this research, in comparison to existing studies, lies firstly in the study by Adietya *et al.,* in 2022 [7], where the propellers used were B4-55 and Ka4-55. In contrast, this study employs B4-70 and Ka4-70 propellers. According to Carlton's book [21], the optimal use of thrust ducts is achieved with these propeller series. Therefore, it is tested without ducts to determine whether it is more optimal compared to other series. Secondly, the use of Sobol fins design is implemented due to Kurt Mizzi's 2017 research [22], which demonstrated a 1.3% increase in efficiency. Thirdly, the turbulence model employs EASM, proven to be superior to RSTM in the study. Lastly, the research involves analyzing the pressure and velocity phenomena of the propeller simultaneously. The analysis is carried out using CFD methods and involves the utilization of the RANSE solver along with an explicit algebraic stress model EASM for turbulence modeling.

2. Methodology

CFD simulation was used to evaluate the propeller performance, which was measured in terms of thrust (K_T) and torque (K_Q) coefficients and efficiency (η_0).

2.1 Modelling

The principal dimensions of the scale model propeller are presented in Table 1, with the type of propeller used was B4-70 and Ka4-70.

One notable outcome was the utilization of Sobol design methodology to choose fins [22] (see Table 2). This approach demonstrated a 1.3% enhancement in overall energy efficiency. This finding established it as a potential benchmark for implementing boss cap fins to enhance the efficiency of the B4-70 propeller.

Table 1
Particular dimension of propeller [23]

Type	Unit	B4-70 and Ka4-70
The number of blades	-	4
Diameter	mm	300
Expanded blade ratio (Ae/Ao)	-	0.7
Pitch diameter ratio		1.2
Angular velocity	rpm	489

Table 2
Sample of Sobol design number 30 [22]

Fin height	Fin length	Pitch	Start angle
0.08 m	0.64 m	28.1°	33,3°

The following are variations of the B4-70 and Ka4-70 propeller models, starting Figure 1 to Figure 3.

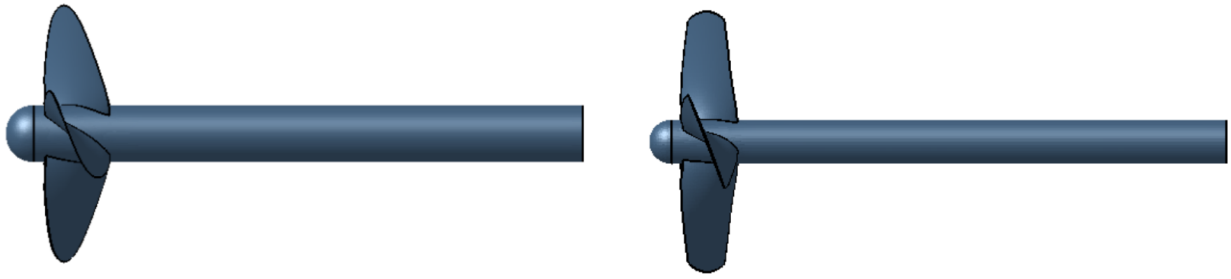

(a) (b)

Fig. 1. Type of propeller: (a) Open propeller B4-70, (b) Open propeller Ka4-70

Type variation involveD the open propeller models B4-70 and Ka4-70 without any additional components such as boss cap fins or nozzles, as shown in Figure 1. This stripped-down configuration serveD as a baseline for the analysis comparison.

The propeller B4-70 model were subjects of intensive investigation aimed at unraveling the complex relationship between design elements and propulsion performance. To gain deeper insights into this dynamic interplay, a diverse array of boss cap fin variations had been employed. These variants encompassed the Default, Straight, Convergent, and Divergent types, each was carefully tailored to discern their specific impact on critical parameters such as K_T, $10K_Q$, and overall η_0. The aim was to determine the values of K_T, $10K_Q$, and η_0 when the B4-70 propeller was combined with various PBCF variations. The significance of these investigations is illustrated in Figure 2, which visually encapsulates the configurations for the Propeller B4-70.

Extensive research was being conducted on the Ka4-70 propeller model to better understand how its design elements affected its performance. Various changes to the boss cap fin had been tested, including Default, Straight, Convergent, and Divergent variations. These changes were designed to investigate their effects on important factors like K_T, $10K_Q$, and overall η_0. The aim was to determine the values of K_T, $10K_Q$, and η_0 when the Ka4-70 propeller was combined with various PBCF variations. The importance of these studies is shown in Figure 3, which provides a visual representation of the different configurations of the Ka4-70 propeller.

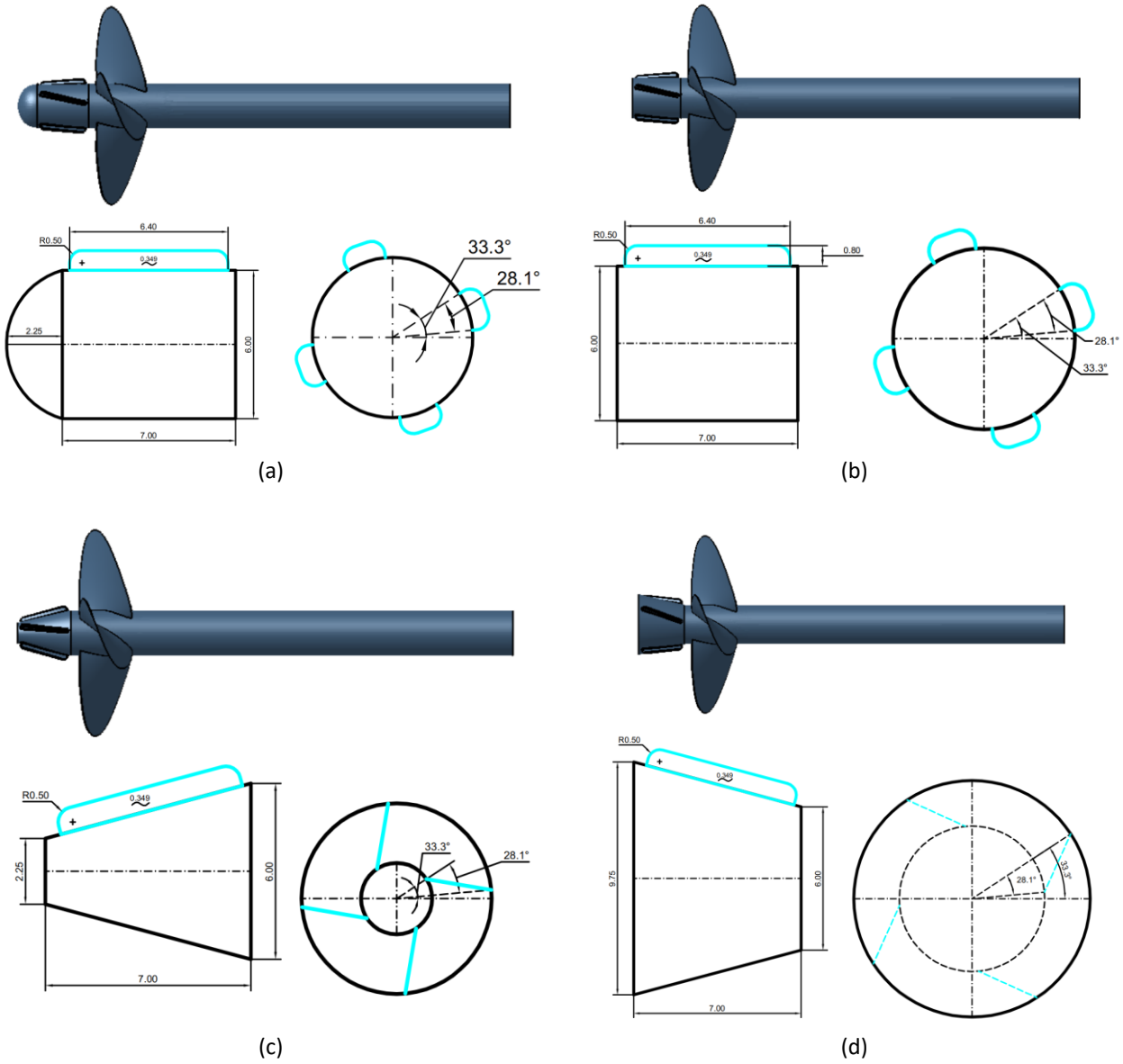

Fig. 2. Type of propeller: (a) Propeller B4-70 BCF default (b) Propeller B4-70 PBCF straight (c) Propeller B4-70 PBCF convergent (d) Propeller B4-70 PBCF divergent

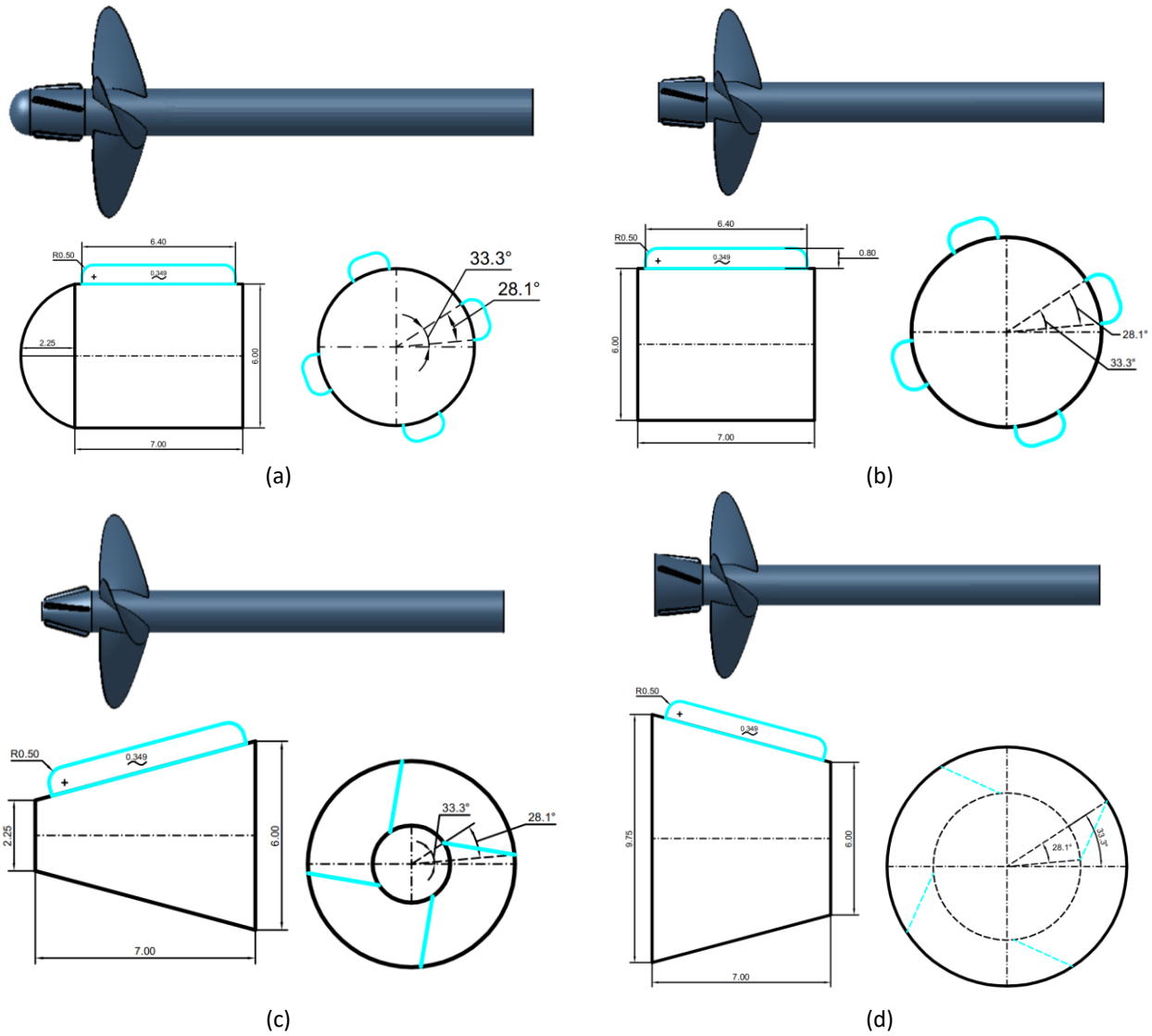

Fig. 3. Types of propeller: (a) Propeller Ka4-70 PBCF default (b) Propeller Ka4-70 PBCF straight (c) Propeller Ka4-70 PBCF convergent (d) Propeller Ka4-70 PBCF divergent

2.2 Numerical Simulation

Numerical simulation was conducted under unsteady conditions using the Reynolds-Averaged Navier-Stokes Equations (RANSE) and the Explicit Algebraic Stress Model (EASM) to address turbulence phenomena [24]. The computational fluid dynamics (CFD) simulation of the PBCF successfully achieved a lower margin of error compared to experimental results. The corresponding equations are presented as Eq. (1), Eq. (2), and Eq. (3), respectively.

$$\frac{\partial \rho}{\partial t} + \frac{\partial (\rho u)}{\partial X} + \frac{\partial (\rho v)}{\partial y} + \frac{\partial (\rho w)}{\partial z} = 0 \tag{1}$$

$$\frac{\partial U_i}{\partial t} + U_j \frac{\partial U_j}{\partial X_j} = \frac{\partial p}{\partial X_i} + \frac{\partial}{\partial X_j}\left[Re_{eff}^{-1}\left(\frac{\partial U_i}{\partial X_j} + \frac{\partial U_j}{\partial X_i}\right)\right] + \frac{1}{2}\left(\frac{\partial U_i}{\partial X_j} + \frac{\partial U_j}{\partial X_i}\right) \tag{2}$$

$$\tau_{IJ} = 2vt\left(S_{ij} - \frac{1}{3}\frac{\delta_{uk}}{\delta_{xk}}\delta_{ij} + \left[a_2 a_4\left(S_{Ik}W_{kj} - W_{ik}S_{kj}\right) - 2_{a3a4}\left(S_{ik}S_{kj} - \frac{1}{3}S_{kl}S_{lk}\delta_{ij}\right)\right]\right) - \frac{2}{3}\rho k\delta_{ij} \tag{3}$$

In the provided equations, u, v, and w represent the flow speed vector field, ρ stands for fluid density, and t denotes time. The Reynolds average velocity components are denoted by Ui = (u, v, w), and the independent coordinate directions are represented by xi = (x, y, z). The mean strain-rate tensor for a body force is indicated by S_i, piezometric pressure is symbolized by p, and effective Reynolds numbers are denoted by Re_{eff}. Eq. (2) models the Reynolds stress using the Explicit Algebraic Stress Model (EASM). The scientific foundation and specific derivation of the EASM can be found in previous studies [15-16]. The final outcome of the Algebraic Reynolds Stress Model for two-dimensional flow is briefly summarized here for clarity. The Reynolds stress tensor is determined using Eq. (3).

The turbulent eddy viscosity, α, and p, can be obtained from Eq. (4), Eq. (5), and Eq. (6) respectively.

$$v_t = \frac{2}{3}k\delta_{IJ} + max(-k_{\alpha 1}, 0.0005\frac{k^2}{\epsilon}) \tag{4}$$

$$(\alpha_1/\tau)^3 + p(\alpha_1/\tau)^2 + q(\alpha_1/\tau) + \mathrm{r} = 0 \tag{5}$$

$$p = -\frac{\gamma_1}{\eta^2\tau^2\gamma_0}, p = \frac{1}{(2\eta^2\tau^2\gamma_0)^2}(\gamma_1^2 - 2\eta^2\tau^2\gamma_0 a_1 - \frac{2}{3}\eta^2\tau^2\alpha_3^2 + 2R^2\eta^2\tau^2\alpha_2^2), \mathrm{r} = \frac{\gamma_1}{(2\eta^2\tau^2\gamma_0)^2} \tag{6}$$

Where τ = k/ϵ is turbulence time scale. Furthermore, it is applied to arrange the Reynold stress into a linear part and a residual part according to Eq. (7):

$$\tau_{ij} = \left(\frac{2}{3}k\delta_{IJ} + 2vtS_{IJ}\right) + \tau_{ij}^r \text{ with } \tau_{ij}^r = \tau_{ij}^{asm} - \frac{2}{3}k\delta_{IJ} + 2vtS_{IJ} \tag{7}$$

Where is τ_{ij}^{asm} obtained from algebraic stress equation (ASM), v_t is eddy viscosity, and k is kinematics, T.

2.3 Boundary Condition

The boundary conditions of the propellers in this research are shown in Figure 4. Boundary condition in the Solid Model is defined as no-slip. The inlet boundary condition is interpreted as the far field. Specified Pressure was used as the boundary condition at the outlet boundary. The Far Field boundary position was applied to the cylindrical surface so that the entire domain was the rotating domain. The rotating frame should be large enough to maintain the Far Field position not affecting the simulation of the flow around the propeller.

The boundary condition termed "far field" was utilized to define the inlet condition, distinct from the "near field." At the outlet boundary, a prescribed pressure was employed as the boundary condition. Within the Solid Model, the boundary condition referred to as "no-slip" was specified. On the cylindrical surface, the far field boundary conditions were imposed to encompass the entire rotating domain. To ensure that the far field boundary did not interfere with the flow prediction around the propeller, the rotating frame must have sufficient size. Meanwhile, the intended domain was a cylinder with a length and diameter of 8D and 6D, respectively, aligning with the axis of symmetry of the propeller. The inlet was situated at a distance of 2D from the model, while the outlet was positioned 6D away from the model.

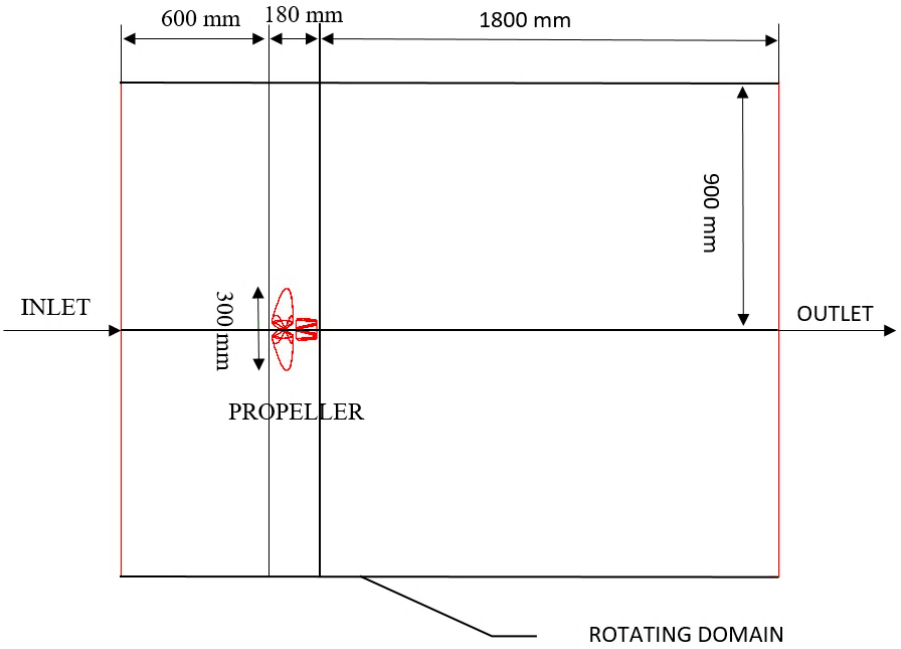

Fig. 4. Boundary condition

2.4 *Grid Generation and Grid Independence Test*

CFD was used to create the mesh structure, as shown in Figure 5. To ensure the reliability of the simulations, a finer mesh was employed [24]. Therefore, it is essential to carry out a study on grid independence. The selection of mesh density should also be balanced with computational time, with a focus on efficiency and optimization [25]. Additionally, the choice of mesh type and its arrangement has a significant impact on the simulation results. Opting for the correct mesh order has been proven to produce better results in CFD simulations. Improving simulation accuracy entails using a finer grid around the model interacting with the fluid, which accurately captures interaction phenomena. Conversely, larger grid sizes can be assigned to distant parts of the fluid to expedite the simulation process. This setup enhances both computational efficiency and result accuracy.

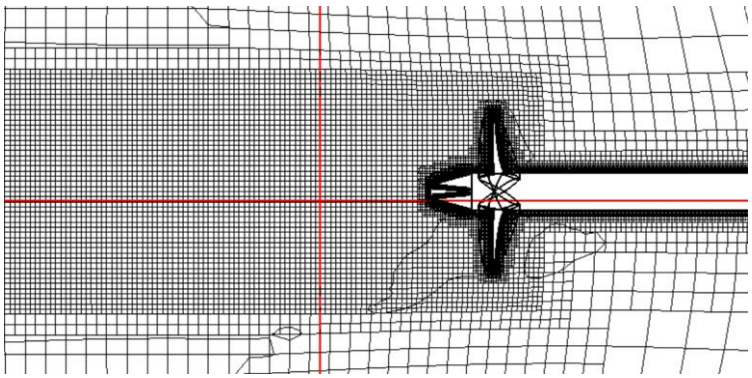

Fig. 5. Meshing of propeller model B4-70 with PBCF convergent

Furthermore, an independent grid was incorporated into several elements to maintain a consistent number that can reduce errors (see Figure 6). When comparing the numerical and experimental data, it was evident that the error rate was less than 2% [26]. However, it is preferable for the value to be less than 0.5% as indicated Table 3.

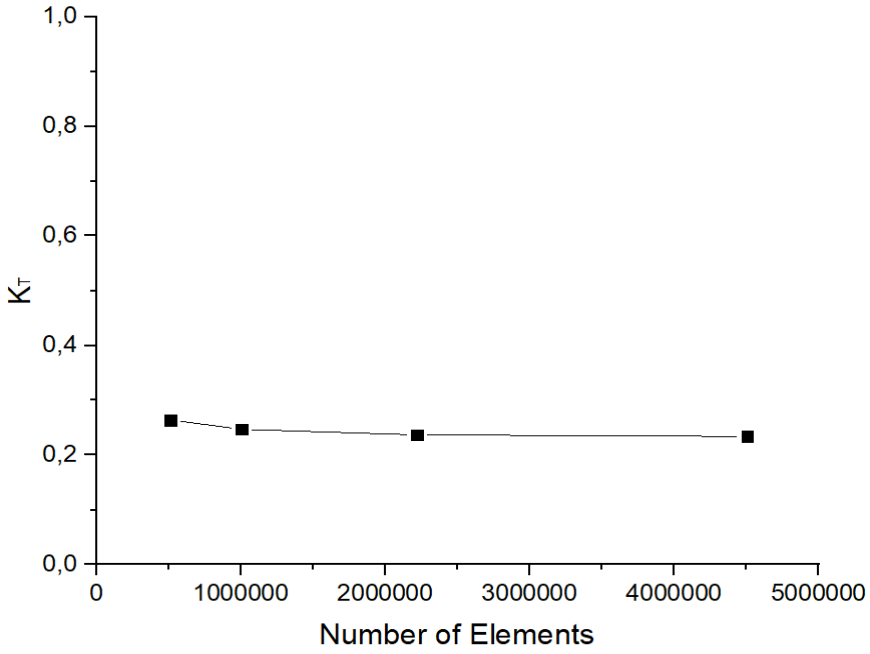

Fig. 6. Grid independence propeller B4-70 with PBCF convergent for K_T

Table 3
Grid independence propeller B4-70 with PBCF convergent

Number of elements	512,798	1,005,782	2,219,443	4,506,342
K_T	0.264	0.247	0.237	0.234
Percentage	-	1.8%	1.0%	0.3%

2.5 Propeller Efficiency

A propeller is typically installed on the stern of a ship to operate effectively in the water encountered during sailing. The ship itself has an impact on the propeller's performance. Therefore, it is necessary to evaluate the propeller's fundamental performance characteristics in open water, independent of the specific ship it is connected to. The performance characteristics of a propeller generally refer to the variations in thrust, torque, and efficiency as the propeller operates at different speeds and rotation rates in open water. To assess the propeller's characteristics in open water, experiments were conducted using model propellers towed in a towing tank. The rotation rate and towing velocity were varied during these experiments to measure the propeller's thrust and torque. The obtained values were then used to calculate non-dimensional parameters such as thrust coefficient (K_T), torque coefficient (K_Q), and open water efficiency (η_0). These parameters were plotted against the advance coefficient (J) on graphs. The formulation for calculating J, K_T, K_Q, and η_0 provided in Eq. (8) – Eq. (11).

$$J = \frac{V_A}{nD} \tag{8}$$

$$K_T = \frac{T}{\rho n^2 D^4} \tag{9}$$

$$K_Q = \frac{Q}{\rho n^2 D^5} \tag{10}$$

$$\eta_0 = \frac{v_a}{2\pi nD}\frac{K_T}{K_Q} \tag{11}$$

3. Open Propeller B4-70 and Ka4-70

The results of the B4-70 open propeller calculation are shown in Figure 7.

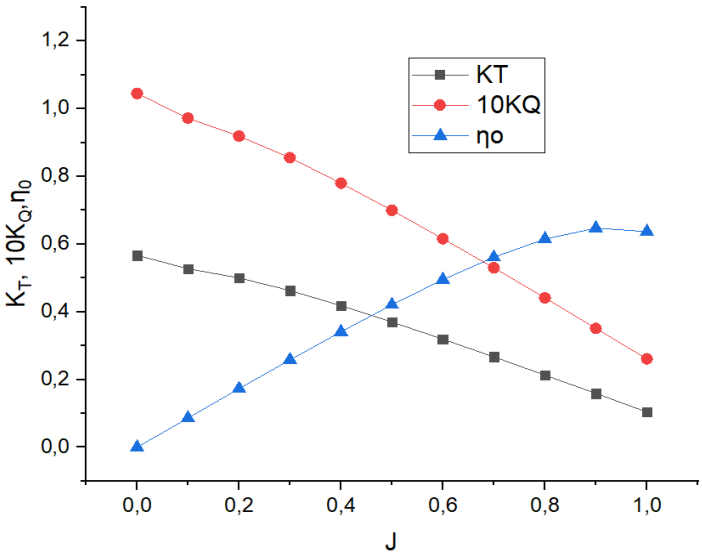

Fig. 7. Open water test diagram for B4-70 open propeller

In the process of creating Figure 7, the open water test graph refers to the experimental graph from Wageningen, where the graph illustrates the values of K_T, $10K_Q$, and efficiency (η0). At J = 0.1, the K_T value of 0.531 decreased, reaching its lowest point at J = 1.0 with a K_T value of 0.104. Similarly, at J = 0.1, the $10K_Q$ value of 0.988 decreased, reaching its lowest point at J = 1.0 with a $10K_Q$ value of 0.261. However, in contrast, the efficiency value had the opposite trend. The efficiency was at its lowest at J = 0.1, increased at J = 0.5 with an efficiency value of 0.421, and peaks at 0.647 at J = 0.9. In conclusion, the open propeller B4-70 operated at high J values, aligning with the needs of a displacement ship [27].

The pressure visualization results for the B4-70 open propeller aligned with the findings from the CFD simulation illustrated in Figure 8. Concerning the boss cap fins, significant pressure was observed at J = 0.1 and J = 0.5, both exceeding 1000 Pa, whereas the pressure value was comparatively lower when J = 0.9, still above 1000 Pa. This study highlighted that the B4-70 propeller, when lacking a PBCF, encountered substantial pressure from low speed (J = 0.1) to medium speed (J = 0.5), indicating a need for a solution to alleviate this pressure issue. The results of the Ka4-70 Naked Propeller calculation are shown in Figure 9.

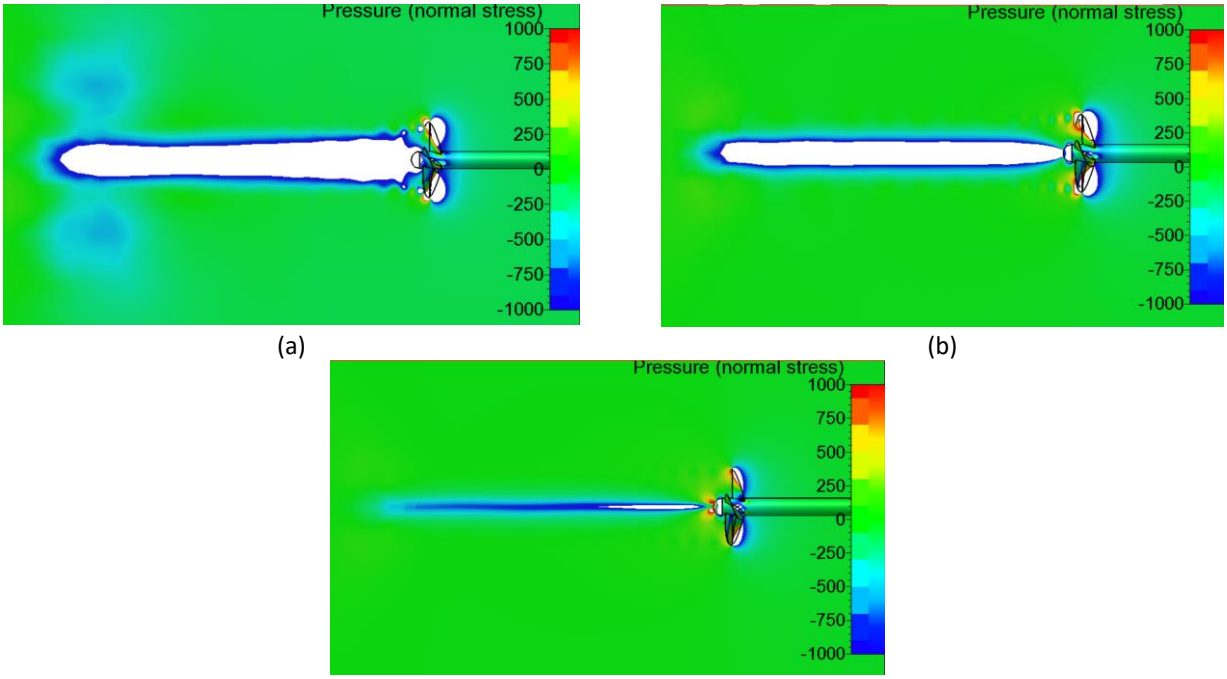

Fig. 8. Visualization of pressure on the B4-70 open propeller (a) Pressure at J = 0.1 (b) Pressure at J = 0.5 (c) Pressure at J = 0.9

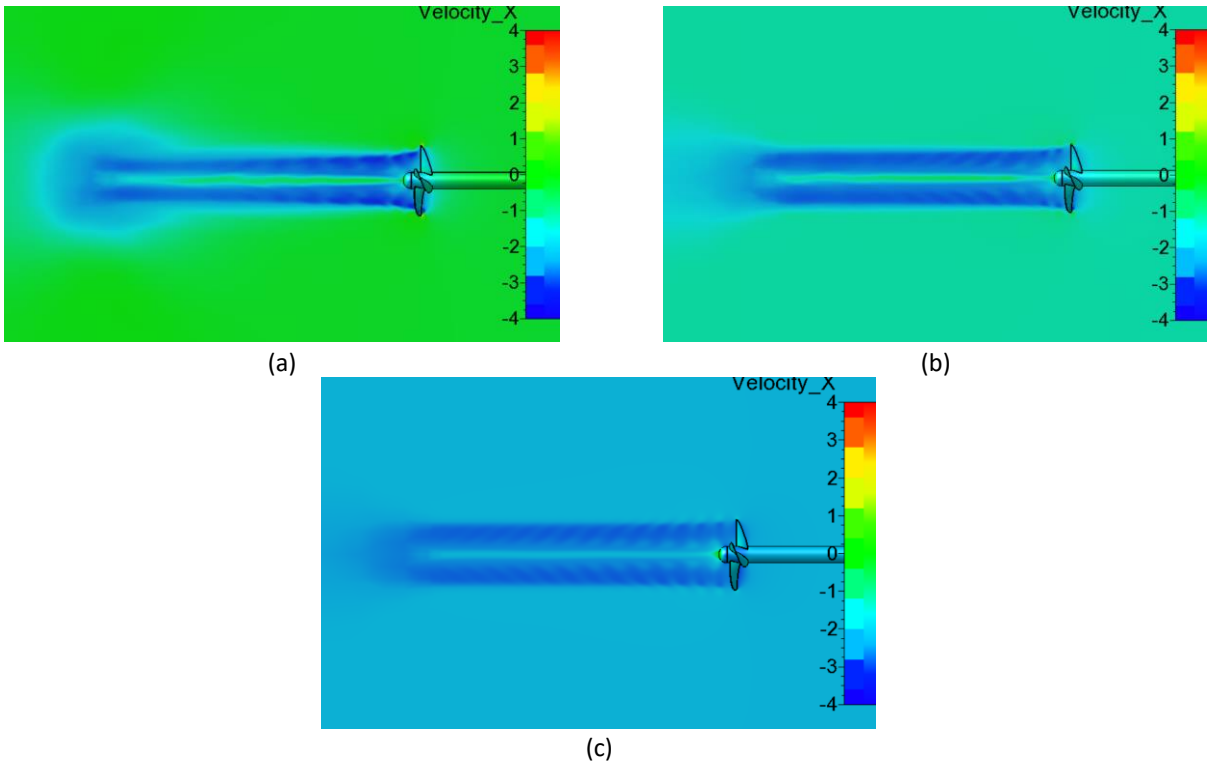

Fig. 9. Visualization of velocity on the open propeller B4-70 (a) Velocity at J = 0.1 (b) Velocity at J = 0.5 (c) Velocity at J = 0.9

The visualization of the velocity of the open propeller B4-70 strengthened the results of the CFD simulation for pressure values. At the boss cap fin, there was a significant pressure when J = 0.1, exceeding 1000 Pa, while at J = 0.5, it remained above 1000 Pa. However, the pressure values were lower when J = 0.9, ranging from 750 to 1000 Pa. In this study, the Open Propeller B4-70 experienced

high pressure at both low and high speeds when J = 0.1 to J = 0.9, indicating a need for solutions to reduce pressure. The visualization of the velocity of the open propeller B4-70 reinforced the CFD simulation results for pressure values. Starting at J = 0.1, the blade section had an axial induced velocity of 3 m/s to 4 m/s, but at the boss cap of the propeller, the flow velocity ranged from 0 m/s to 1 m/s. Meanwhile, at J = 0.5, the axial induced velocity on the blade section was 3 m/s to 4 m/s, and at the boss cap of the propeller, there was flow with velocities ranging from 0 m/s to 2 m/s. When J = 0.9, the blade's axial induced velocity is 3 m/s to 4 m/s, even though there was an increase in flow velocity at the boss cap of the propeller, ranging from 0 m/s to 3 m/s. In conclusion, for the B4-70 Naked propeller, as the J value (advanced coefficient) increased, the flow velocity at the boss cap also increased, while the flow velocity at the propeller blade remained the same. Therefore, solutions are needed to address the increase in flow velocity at the boss cap.

In the process of creating Figure 10, the open water test graph refers to the experimental graph from Wageningen, where the graph illustrates the values of K_T, $10K_Q$, and Efficiency (η0). At J = 0.1, the K_T value of 0.549 decreased, reaching its lowest point at J = 1.0 with a K_T value of 0.105. Similarly, at J = 0.1, the $10K_Q$ value of 1.032 decreased, reaching its lowest point at J = 1.0 with a $10K_Q$ value of 0.289. However, in contrast, the efficiency value had the opposite trend. The efficiency was at its lowest at J = 0.1, increased at J = 0.5 with an efficiency value of 0.419, and peaked at 0.608 at J = 0.9 [28].

The pressure visualization outcomes for the Ka4-70 propeller in the absence of a Nozzle and PBCF were consistent with the data derived from the CFD simulation as outlined in Figure 11. In the boss cap area, substantial pressure was observed at J = 0.1, J = 0.5, and J = 0.7, all exceeding the threshold of 1000 Pa. This study underscored that the Ka4-70 propeller, when not equipped with a Nozzle and PBCF, encountered notable pressure starting from low speeds (J = 0.1) up to high speeds (J = 0.7). Previous investigations into open propellers also revealed similar instances of high pressure.

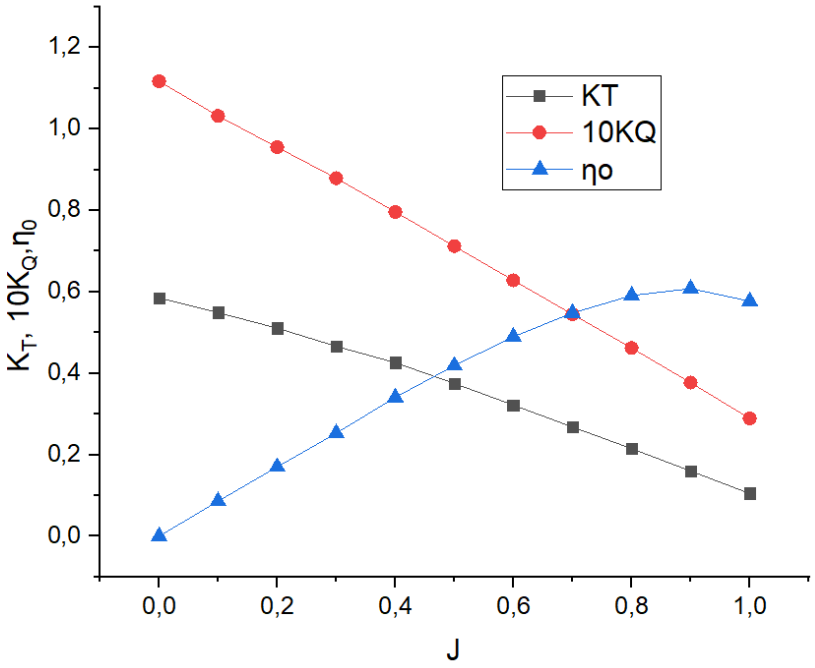

Fig. 10. Open water test diagram for Ka4-70 open propeller

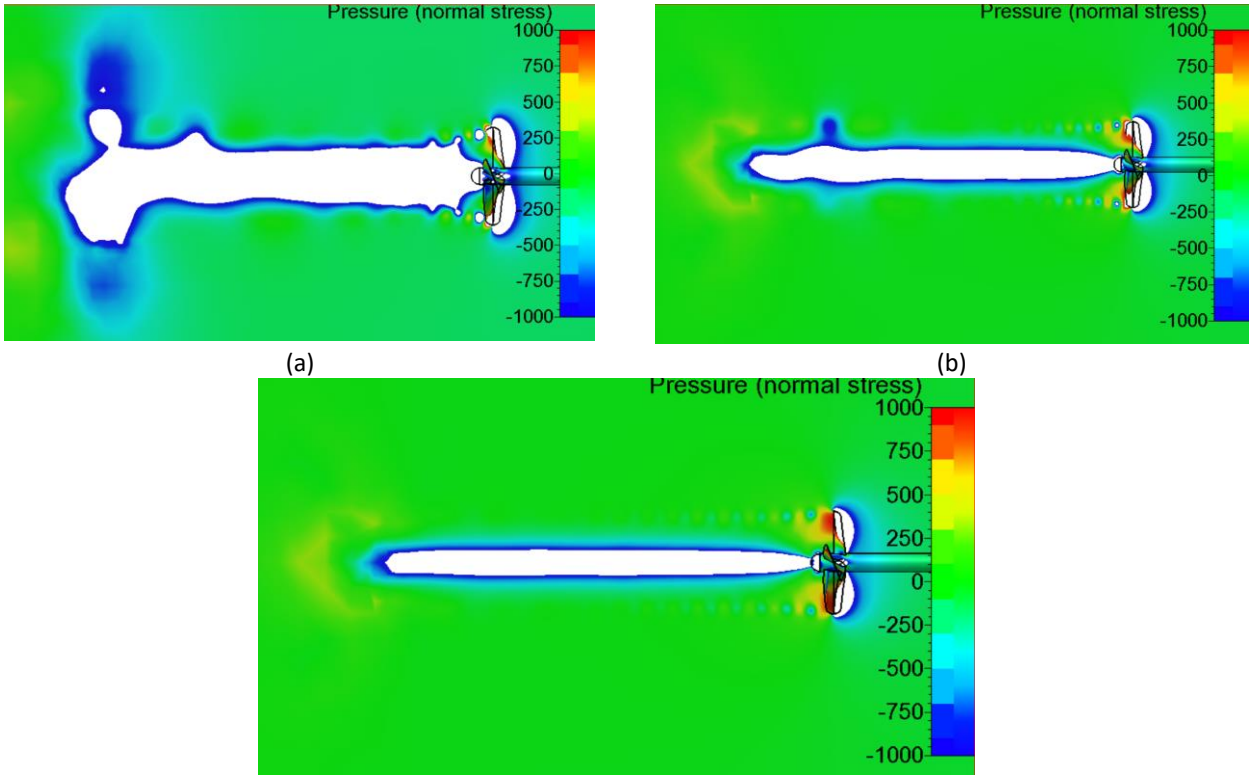

Fig. 11. Visualization of pressure on the Ka4-70 open propeller (a) Pressure open propeller at J = 0.1 (b) Pressure open propeller at J = 0.5 (c) Pressure open propeller at J = 0.7

The visualization of the velocity of the open propeller Ka4-70 reinforced the results of the CFD simulation for pressure values, shown in Figure 12. At the boss cap fin, there was a significant pressure when J = 0.1, exceeding 1000 Pa, while at J = 0.5, it remained above 1000 Pa. However, the pressure values were lower when J = 0.7, also exceeding 1000 Pa. In this study, the open propeller Ka4-70 experienced high pressure at low speeds (J = 0.1) up to moderate speeds (J = 0.7), indicating a need for solutions to reduce pressure. The visualization of the velocity of the open propeller Ka4-70 reinforced the CFD simulation results for pressure values. Starting at J = 0.1, the blade section had an axial induced velocity of 3 m/s to 4 m/s, but at the boss cap of the propeller, the flow velocity ranged from 0 m/s to 1 m/s. Meanwhile, at J = 0.5, the axial induced velocity on the blade section was 3 m/s to 4 m/s, and at the boss cap of the propeller, there was flow with velocities ranging from 0 m/s to 2 m/s. When J = 0.7, the blade's axial induced velocity was 3 m/s to 4 m/s, even though there was an increase in flow velocity at the boss cap of the propeller, ranging from 0 m/s to 3 m/s. In conclusion, for the open propeller Ka4-70, as the J value (advanced coefficient) increased, the flow velocity at the boss cap also increased, while the flow velocity at the propeller blade remained the same. Therefore, solutions are needed to address the increase in flow velocity at the boss cap.

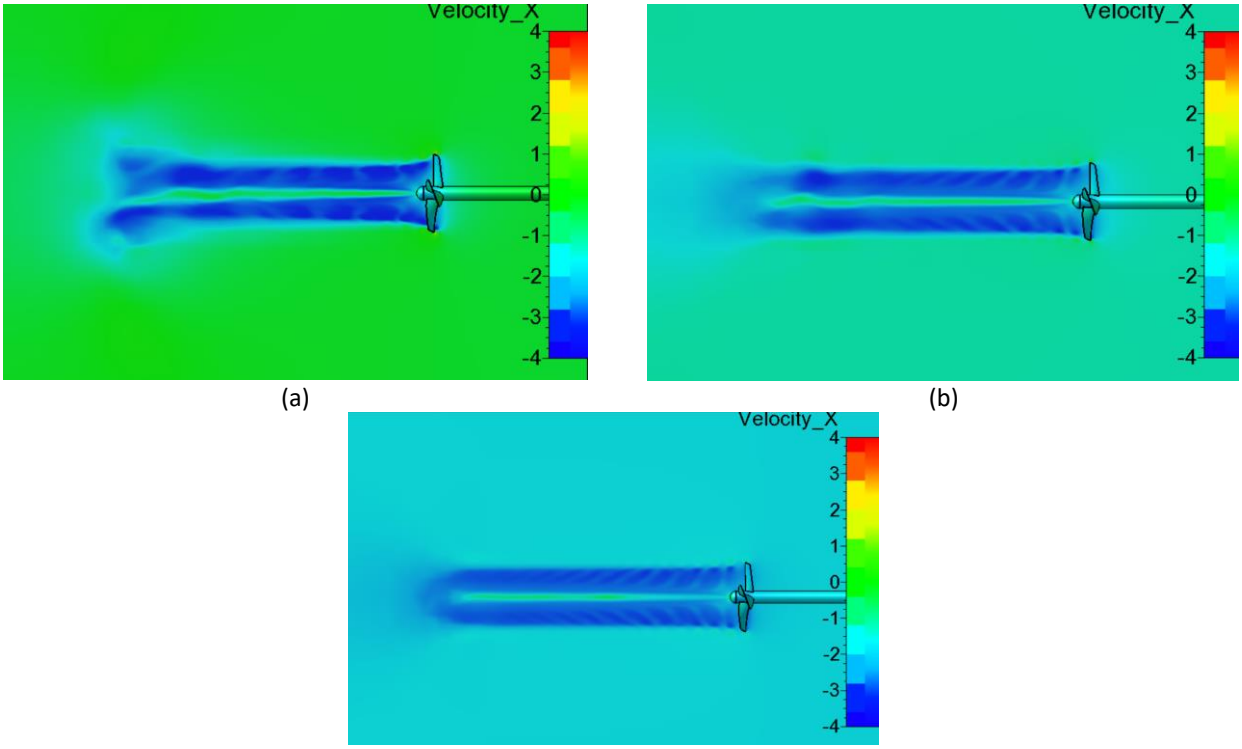

Fig. 12. Visualization of velocity on the open propeller Ka4-70 (a) Velocity at J = 0.1 (b) Velocity at J = 0.5 (c) Velocity at J = 0.7

4. Propeller B4-70 and Ka4-70 with PBCF

4.1 Propeller B4-70 with PBCF

In the process of creating Figure 13, the open water test graph refers to the experimental graph from Wageningen, where the graph illustrates the values of K_T, $10K_Q$, and Efficiency ($\eta 0$). Meanwhile, at J = 0.1, the K_T value of 0.533 decreased, reaching its lowest point at J = 1.0 with a K_T value of 0.118. Similarly, at J = 0.1, the $10K_Q$ value of 0.975 decreased, reaching its lowest point at J = 1.0 with a $10K_Q$ value of 0.282. However, in contrast, the efficiency value had the opposite trend. The efficiency was at its lowest at J = 0.1, increased at J = 0.5 with an efficiency value of 0.424, and peaked at 0.665 at J = 1.0. In conclusion, the B4-70 propeller with default boss cap fins operates at high J values, akin to the usage in displacement ships [29].

The results of propeller B4-70 with PBCF calculation are shown in Figure 13.

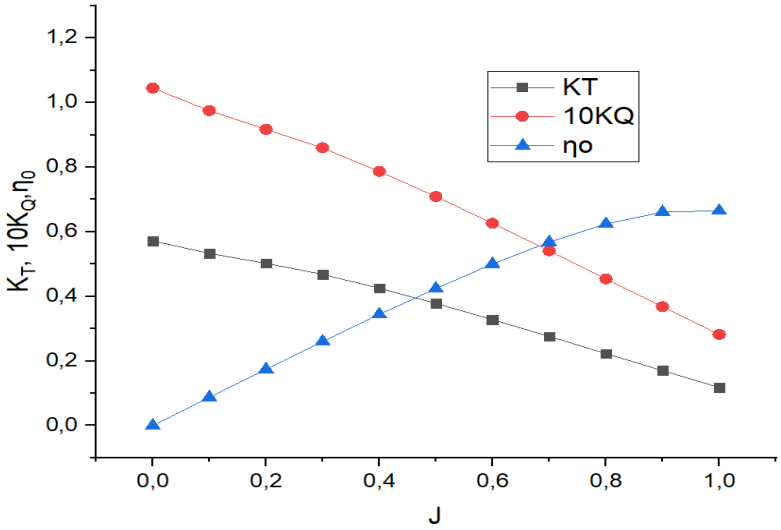

Fig. 13. Open water test diagram of B4-70 PBCF default

In the visualization of the pressure on the B4-70 open propeller, the results from the CFD simulation are corroborated in Figure 14. In the region of the boss cap fins, significant pressure occurred at J = 0.1, exceeding 1000 Pa; similarly, at J = 0.5, the pressure is also above 1000 Pa, but the pressure value was lower when J = 0.9, ranging from 500 to 750 Pa. In this study, the B4-70 open propeller experienced substantial pressure at low speeds, J = 0.1, up to moderate speeds, J = 0.5.

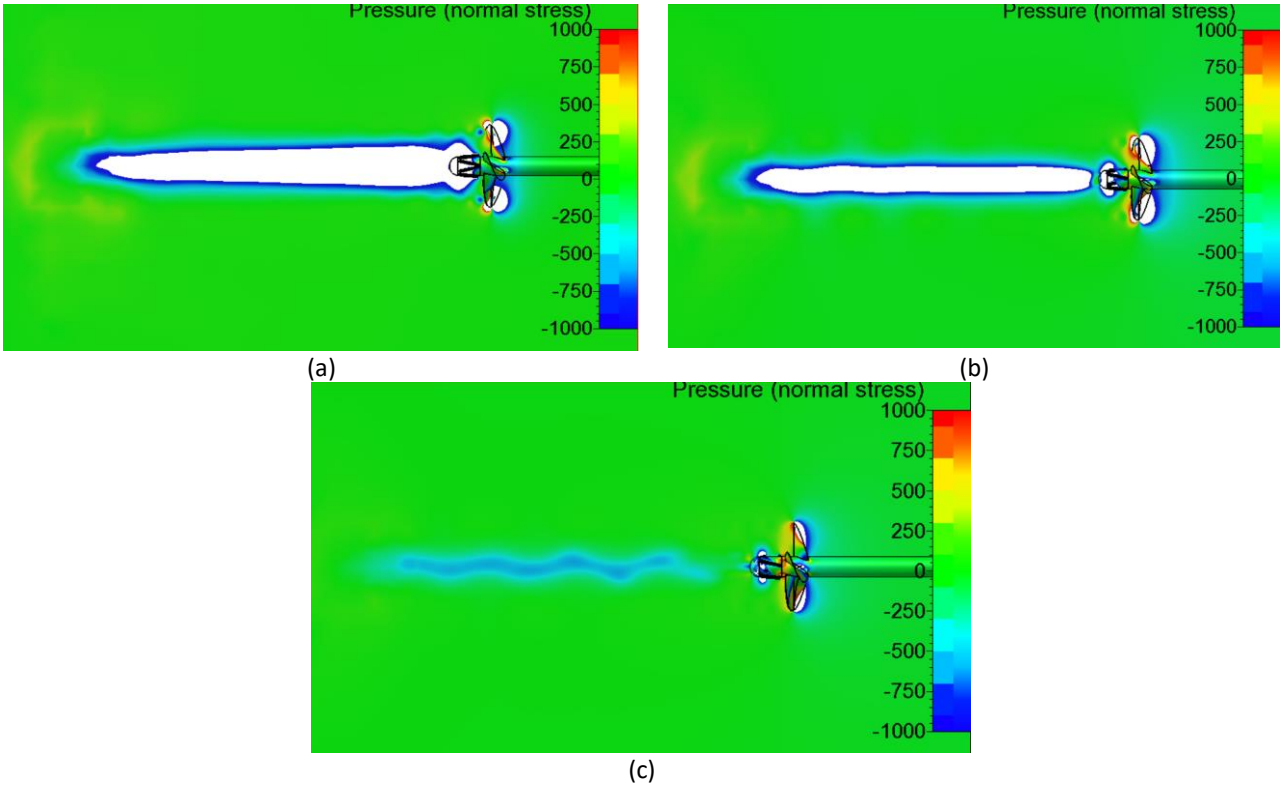

Fig. 14. Visualization of the pressure on the B4-70 propeller with PBCF default (a) Pressure at J = 0.1 (b) Pressure at J = 0.5 (c) Pressure at J = 0.9

The visualization of the velocity of the propeller B4-70 with BCF Default strengthened the results of the CFD simulation for pressure values, shown in Figure 15. At the boss cap fin, there was a significant pressure when J = 0.1, exceeding 1000 Pa, while at J = 0.5, it remained above 1000 Pa. However, the pressure values were lower when J = 0.9, ranging from 500 Pa to 750 Pa. In this study, the propeller B4-70 without PBCF experienced high pressure at low speeds (J = 0.1) up to moderate speeds (J = 0.5), indicating a need for solutions to reduce pressure. The visualization of the velocity of the propeller B4-70 with BCF Default reinforced the CFD simulation results for pressure values. Starting at J = 0.1, the blade section had an induced axial velocity of 3 m/s to 4 m/s, but at the boss cap of the propeller, the flow velocity was 3 m/s to 4 m/s. Meanwhile, at J = 0.5, the axial induced velocity on the blade section was 3 m/s to 4 m/s, and at the boss cap of the propeller, there was flow with velocities ranging from 2 m/s to 3 m/s. When J = 0.9, the blade's induced axial velocity was 3 m/s to 4 m/s, even though there was an increase in flow velocity at the boss cap of the propeller, ranging from 0 m/s to 2 m/s. In conclusion, for the propeller B4-70 with BCF Default, as the J value (advanced coefficient) increased, the flow velocity at the boss cap fins decreased, while the flow velocity at the propeller blade remained the same.

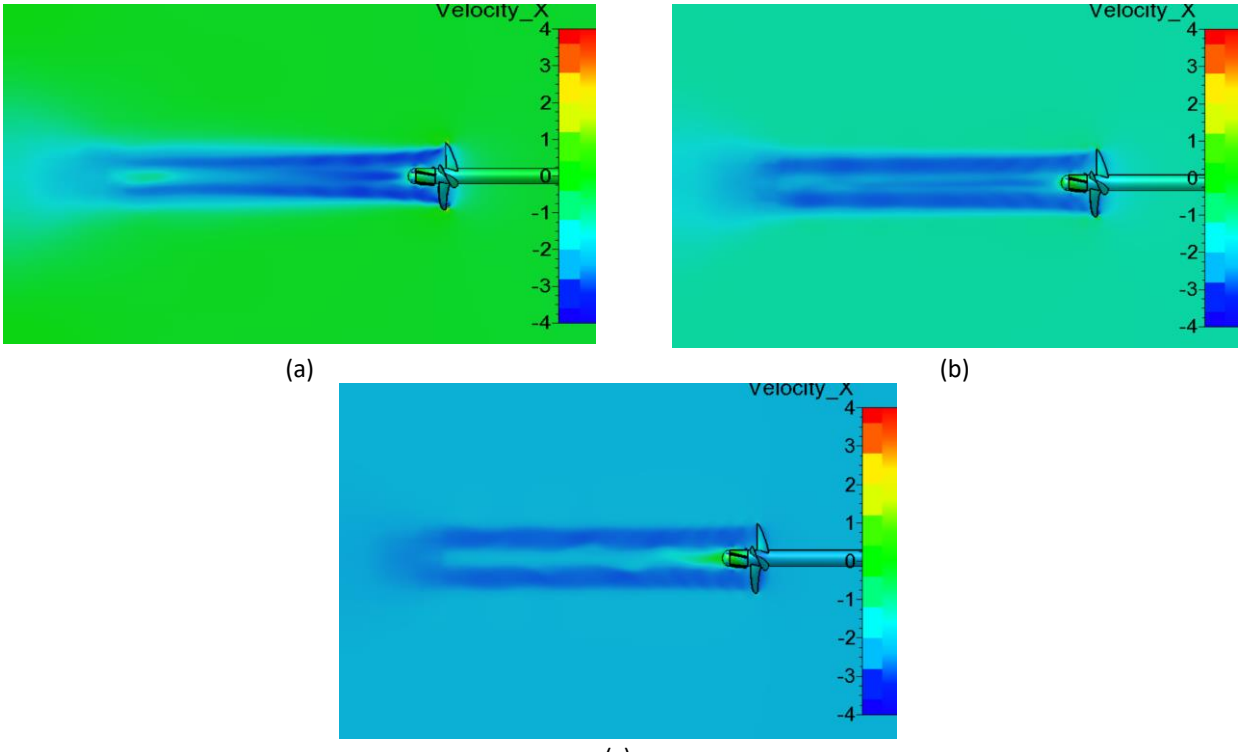

Fig. 15. Visualization of velocity on the open propeller B4-70 with PBCF default (a) Velocity at J = 0.1 (b) Velocity at J = 0.5 (c) Velocity at J = 0.9

The results of propeller B4-70 with PBCF Straight calculation are shown in Figure 16.

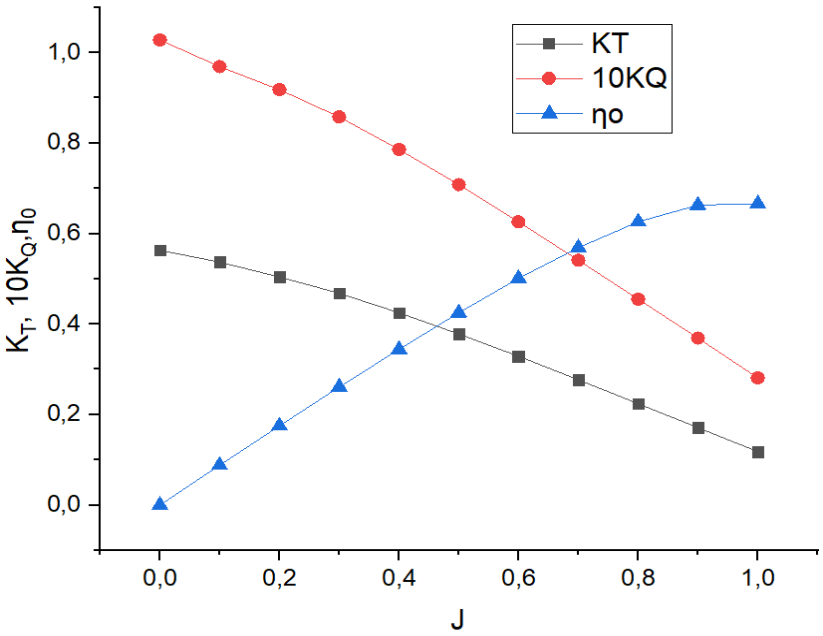

Fig. 16. Open water test diagram of B4-70 PBCF straight

In the process of creating Figure 16, the open water test graph refers to the experimental graph from Wageningen, where the graph illustrates the values of K_T, $10K_Q$, and efficiency (η0). Meanwhile, at J = 0.1, the K_T value of 0.537 decreased, reaching its lowest point at J = 1.0 with a K_T value of 0.118. Similarly, at J = 0.1, the $10K_Q$ value of 0.969 decreased, reaching its lowest point at J = 1.0 with a $10K_Q$ value of 0.281. However, in contrast, the efficiency value had the opposite trend. The efficiency was at its lowest at J = 0.1, increased at J = 0.5 with an efficiency value of 0.425, and peaked at 0.666 at J = 1.0. In conclusion, the B4-70 propeller with straight-type boss cap fins was well-suited for use on displacement ships operating above J = 0.5 [30].

In the visualization of the pressure on the B4-70 propeller with Straight Boss Cap Fins, the results from the CFD simulation were reinforced by Figure 17. In the region of the straight boss cap fins, significant pressure occurred at J = 0.1, exceeding 1000 Pa; similarly, at J = 0.5, the pressure was also above 1000 Pa, but the pressure value was lower when J = 0.9, ranging from 500 to 750 Pa. In this study, the B4-70 open propeller experienced substantial pressure at low speeds, J = 0.1, up to moderate speeds, J = 0.5, indicating a need for a solution to reduce the pressure.

The visualization of the velocity of the propeller B4-70 with BCF Straight reinforced the results of the CFD simulation for pressure values, shown in Figure 18. At the boss cap fin, there was a significant pressure when J = 0.1, exceeding 1000 Pa, while at J = 0.5, it remained above 1000 Pa. However, the pressure values were lower when J = 0.9, ranging from 500 Pa to 750 Pa. In this study, the propeller B4-70 with BCF Straight experienced high pressure at low speeds (J = 0.1) up to moderate speeds (J = 0.5), indicating a need for solutions to reduce pressure. The visualization of the velocity of the propeller B4-70 with BCF Straight reinforced the CFD simulation results for pressure values. Starting at J = 0.1, the blade section had an induced axial velocity of 3 m/s to 4 m/s, but at the boss cap of the propeller, the flow velocity ranged from 0 m/s to 4 m/s. Meanwhile, at J = 0.5, the axial induced velocity on the blade section was 3 m/s to 4 m/s, and at the boss cap of the propeller, there was flow with velocities ranging from 0 m/s to 3 m/s. When J = 0.9, the blade's induced axial velocity was 3 m/s to 4 m/s, even though there was an increase in flow velocity at the boss cap of the propeller, ranging from 0 m/s to 2 m/s. In conclusion, for the propeller B4-70 with BCF Straight, as the J value (advanced coefficient) increased, the flow velocity at the boss cap increases [24], while the flow

velocity at the propeller blade remained the same. Therefore, solutions are needed to address the increase in flow velocity at the boss cap.

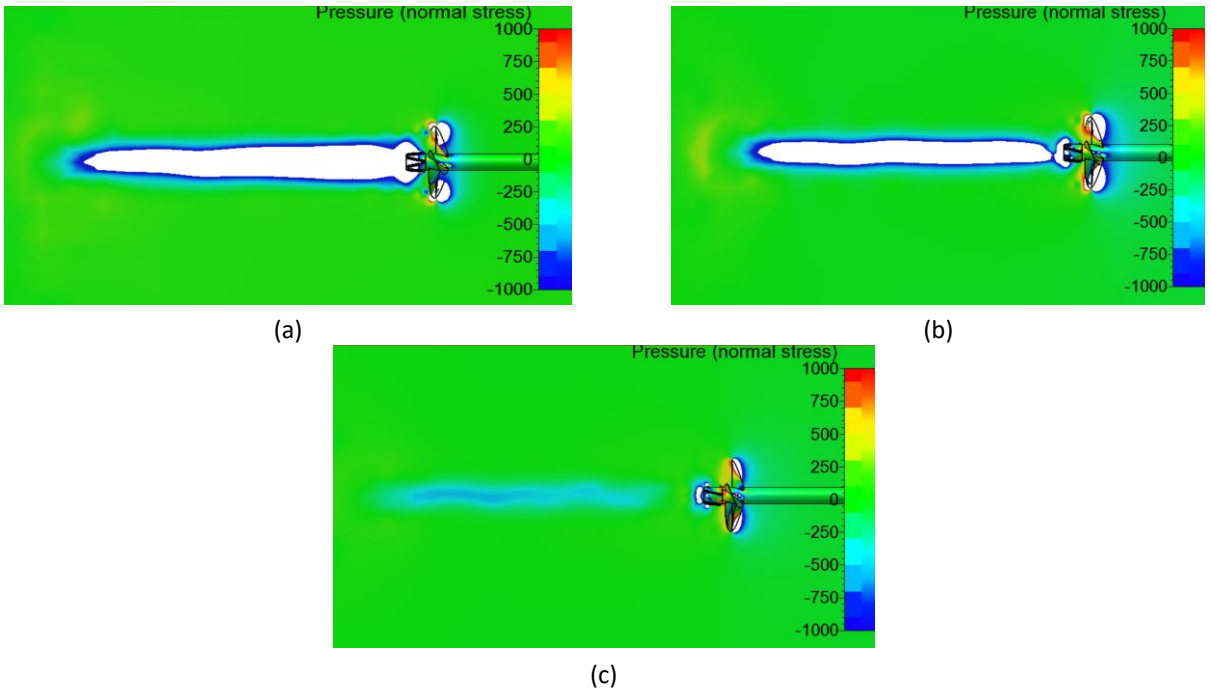

Fig. 17. Visualization of pressure on the B4-70 propeller with PBCF straight (a) Pressure at J = 0.1 (b) Pressure at J = 0.5 (c) Pressure at J = 0.9

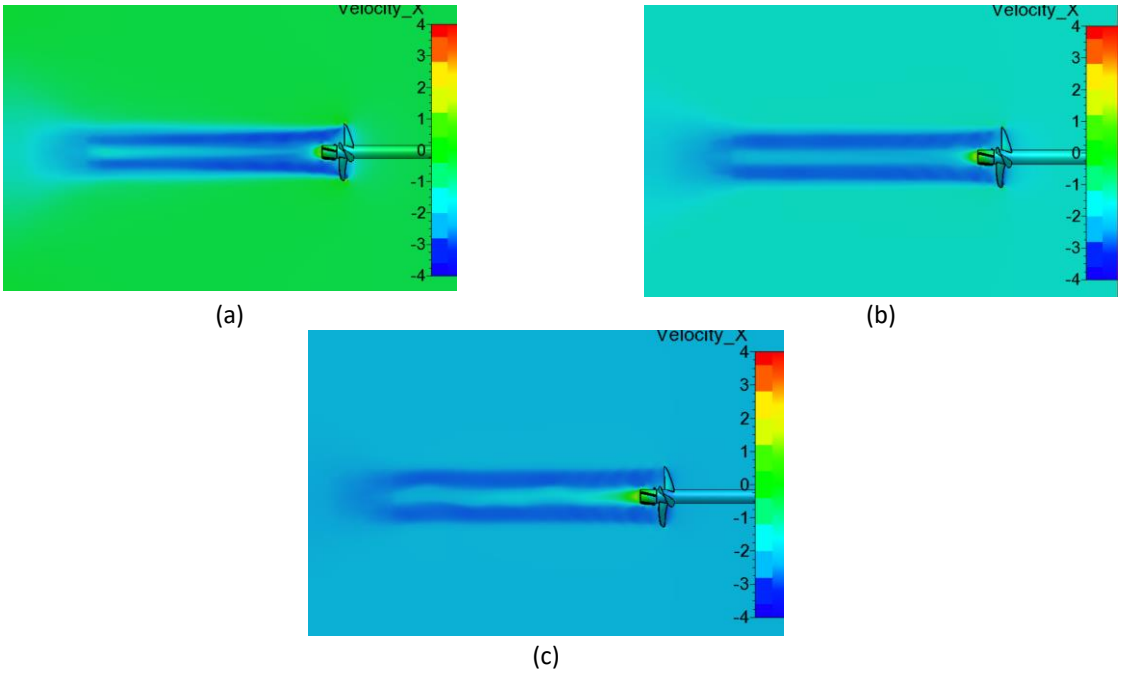

Fig. 18. Visualization of velocity on the B4-70 propeller with PBCF straight (a) Velocity at J = 0.1 (b) Velocity at J = 0.5 (c) Velocity at J = 0.9

The results of propeller B4-70 with PBCF Convergent calculation are shown in Figure 19.

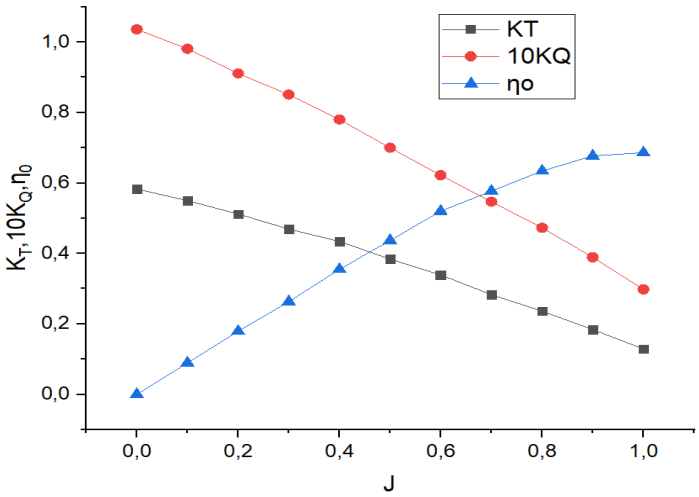

Fig. 19. Open water test diagram of B4-70 PBCF convergent

In the process of creating Figure 19, the open water test graph refers to the experimental graph from Wageningen, where the graph illustrates the values of K_T, $10K_Q$, and efficiency (η0). Consequently, at J = 0.1, the K_T value of 0.550 decreased, reaching its lowest point at J = 1.0 with a K_T value of 0.129. Similarly, at J = 0.1, the $10K_Q$ value of 0.981 decreased, reaching its lowest point at J = 1.0 with a $10K_Q$ value of 0.298. However, in contrast, the efficiency value had the opposite trend. The efficiency was at its lowest at J = 0.1, increased at J = 0.5 with an efficiency value of 0.437, and peaked at 0.686 at J = 1.0. The study on the B4-70 propeller with convergent-type boss cap fins concludes that this propeller can be used optimally on ships.

The pressure visualization of the B4-70 propeller with straight boss cap fins reinforced the outcomes of the CFD simulation as presented in Figure 20. In the area of the boss cap fins, notable pressure was observed at J = 0.1 and J = 0.5, both surpassing 1000 Pa, while the pressure value was relatively lower at J = 0.9, exceeding 500 Pa. This study revealed that the B4-70 Propeller with straight boss cap fins encountered significant pressure at low speeds (J = 0.1) up to J = 0.5 [27].

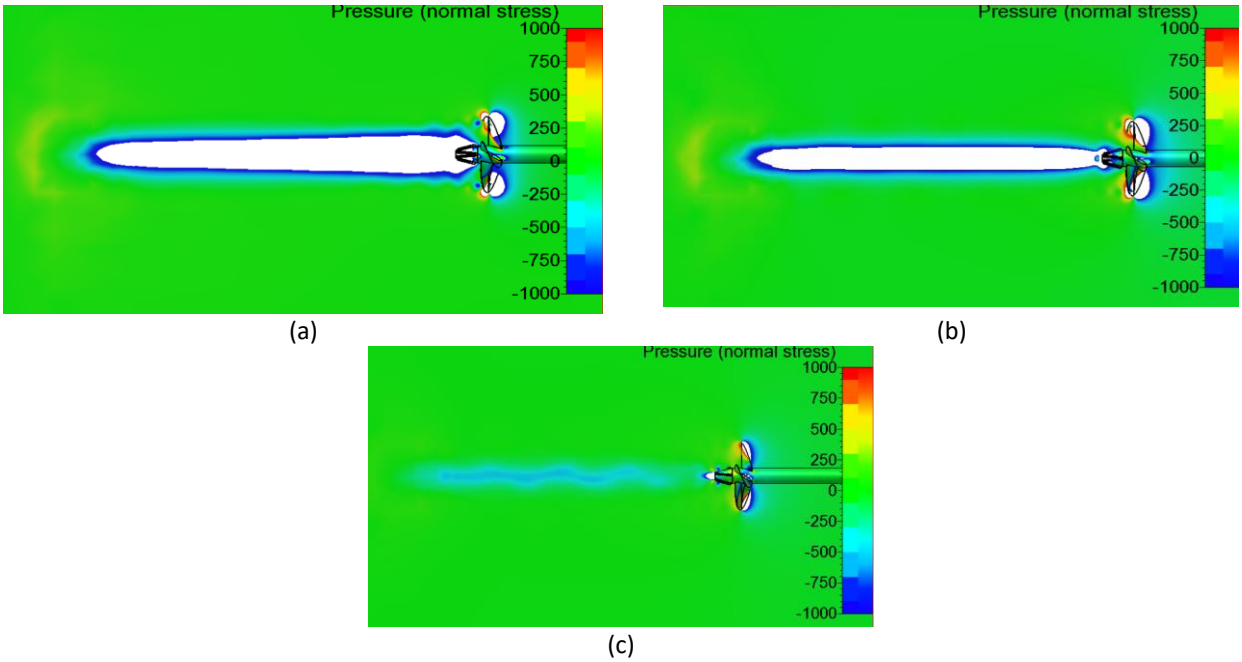

Fig. 20. Visualization of pressure propeller B4-70 with PBCF convergent (a) pressure at J = 0.1 (b) pressure at J = 0.5 (c) Pressure at J = 0.9

The visualization of the velocity of propeller B4-70 with BCF Convergent strengthened the results of the CFD simulation for pressure values, shown in Figure 21. At the boss cap fin, there was significant pressure when J = 0.1, exceeding 1000 Pa, while at J = 0.5, it remained above 1000 Pa. However, the pressure values were lower when J = 0.9, also exceeding 1000 Pa. In this study, the propeller B4-70 without PBCF experienced high pressure at low speeds (J = 0.1) up to moderate speeds (J = 0.5), indicating a need for solutions to reduce pressure. The visualization of the velocity of propeller B4-70 with BCF Convergent reinforced the CFD simulation results for pressure values. Starting at J = 0.1, the blade section had an induced axial velocity of 3 m/s to 4 m/s, but at the boss cap of the propeller, the flow velocity was 3 m/s to 4 m/s. Meanwhile, at J = 0.5, the axial induced velocity on the blade section was 3 m/s to 4 m/s, and at the boss cap of the propeller, there was flow with velocities ranging from 3 m/s to 4 m/s. When J = 0.9, the blade's induced axial velocity was 3 m/s to 4 m/s, even though there was an increase in flow velocity at the boss cap of the propeller, ranging from 0 m/s to 1 m/s. In conclusion, for the propeller B4-70 with BCF Convergent, as the J value (advanced coefficient) increased, the flow velocity at the boss cap increased, while the flow velocity at the propeller blade remained the same. Therefore, solutions are needed to address the increase in flow velocity at the boss cap.

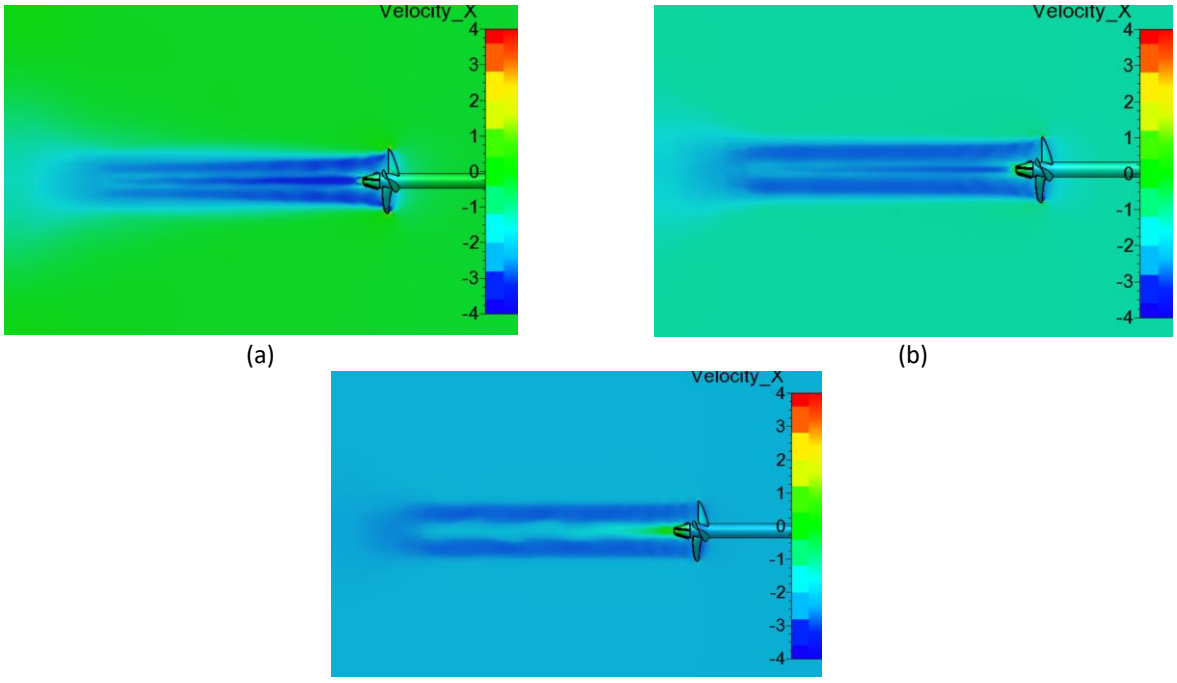

Fig. 21. Visualization of velocity on the B4-70 propeller with PBCF convergent (a) Velocity at J = 0.1 (b) Velocity at J = 0.5 (c) Velocity at J = 0.9

The results of propeller B4-70 with PBCF Divergent calculation are shown in Figure 22.

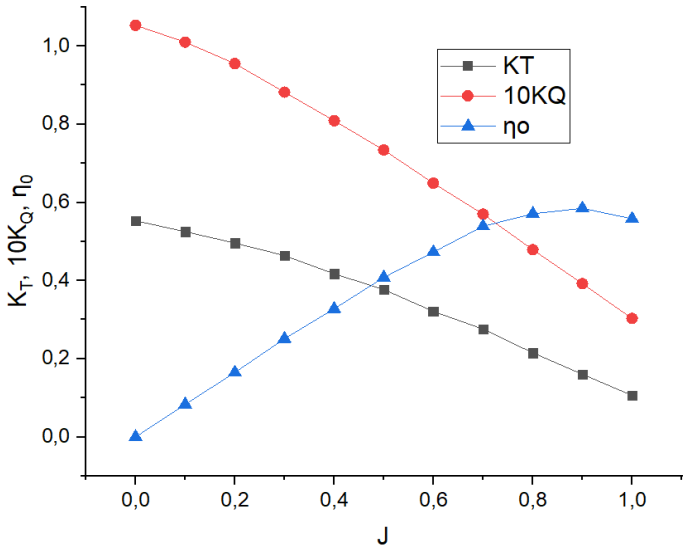

Fig. 22. Open water test diagram of B4-70 PBCF divergent

In the process of creating Figure 22, the open water test graph refers to the experimental graph from Wageningen, where the graph illustrates the values of K_T, $10K_Q$, and Efficiency (η0). Although, at J = 0.1, the K_T value of 0.525 decreased, reaching its lowest point at J = 1.0 with a K_T value of 0.106. Similarly, at J = 0.1, the $10K_Q$ value of 1.010 decreased, reaching its lowest point at J = 1.0 with a $10K_Q$ value of 0.303. However, in contrast, the efficiency value had the opposite trend. The efficiency was at its lowest at J = 0.1, increased at J = 0.5 with an efficiency value of 0.408, and peaked at 0.585 at J = 0.9. For the B4-70 propeller with divergent-type boss cap fins, it was not highly recommended for use on displacement ships as there was a decrease in thrust and efficiency values at high J values.

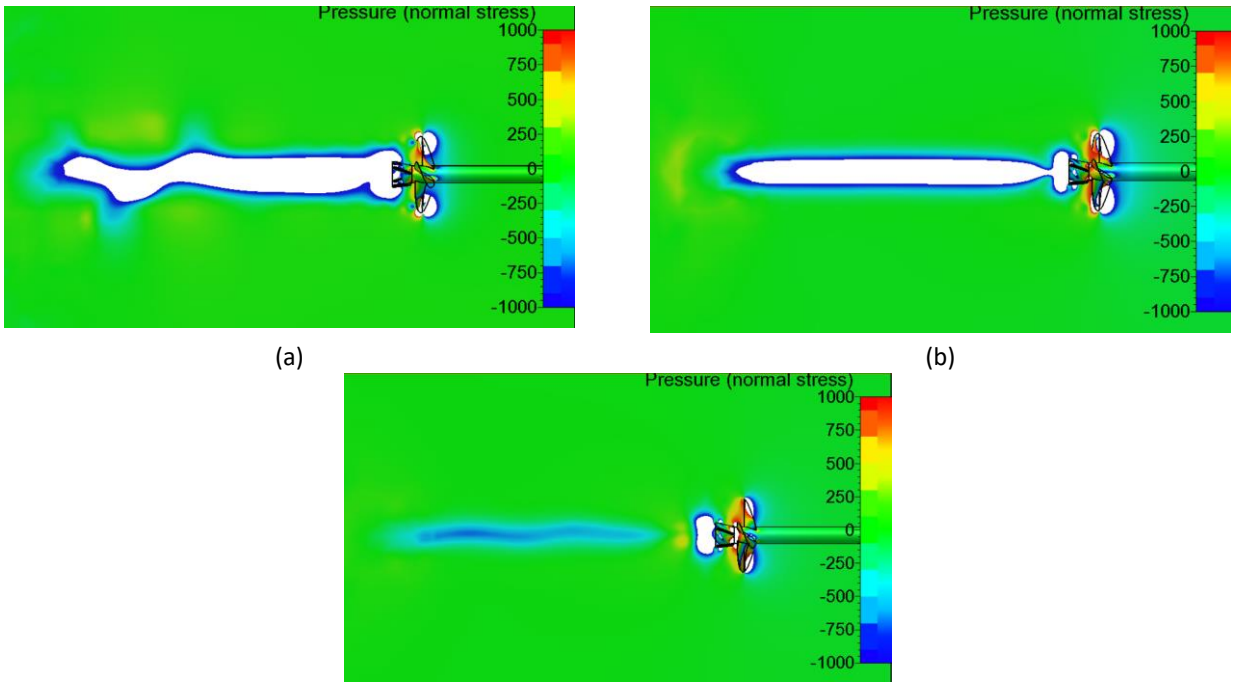

Fig. 23. Visualization of pressure on the B4-70 propeller with PBCF divergent (a) Pressure at J = 0.1 (b) Pressure at J = 0.5(c) Pressure at J = 0.9

The visualization of pressure on the B4-70 propeller with Divergent Boss Cap Fins reinforced the results of the CFD simulation in Figure 23. In the region of the divergent boss cap fins, significant pressure occurred at J = 0.1, exceeding 1000 Pa; similarly, at J = 0.5, the pressure was also above 1000 Pa, but the pressure value was lower when J = 0.9, ranging from 500 to ≥1000 Pa. This study highlights that the B4-70 open propeller experienced substantial pressure at low speeds, J = 0.1, up to high speeds, J = 0.9 [29].

The visualization of the velocity of propeller B4-70 with BCF Divergent reinforced the results of the CFD simulation for pressure values, shown in Figure 24. At the boss cap fin, there was a significant pressure when J = 0.1, exceeding 1000 Pa, while at J = 0.5, it remained above 1000 Pa. However, the pressure values were lower when J = 0.9, ranging from 500 Pa to ≥1000 Pa. In this study, the propeller B4-70 with BCF Divergent experienced high pressure at low speeds (J = 0.1) up to high speeds (J = 0.9), indicating a need for solutions to reduce pressure. The visualization of the velocity of propeller B4-70 with BCF Divergent reinforced the CFD simulation results for pressure values. Starting at J = 0.1, the blade section had an induced axial velocity of 3 m/s to 4 m/s, but at the boss cap of the propeller, the flow velocity ranged from 0 m/s to 3 m/s. Meanwhile, at J = 0.5, the axial induced velocity on the blade section was 3 m/s to 4 m/s, and at the boss cap of the propeller, there was flow with velocities ranging from 0 m/s to 3 m/s. When J = 0.9, the blade's induced axial velocity was 3 m/s to 4 m/s, even though there was an increase in flow velocity at the boss cap of the propeller, ranging from 0 m/s to 2 m/s. In conclusion, for the propeller B4-70 with BCF Divergent, as the J value (advanced coefficient) increased, the flow velocity at the boss cap increased, while the flow velocity at the propeller blade remained the same. Therefore, solutions are needed to address the increase in flow velocity at the boss cap.

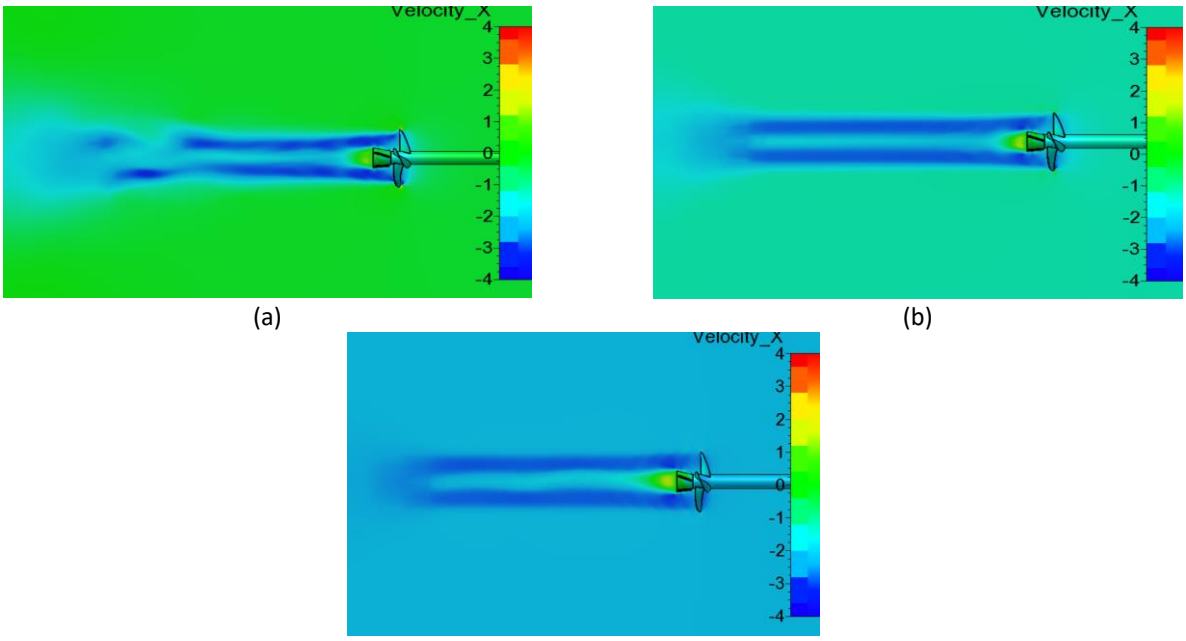

Fig. 24. Visualization of velocity on the B4-70 propeller with PBCF divergent (a) Velocity at J = 0.1 (b) Velocity at J = 0.5 (c) Velocity at J = 0.9

4.2 The Propeller Ka4-70 with PBCF

The results of Propeller Ka4-70 with PBCF Default calculation are shown in Figure 25.

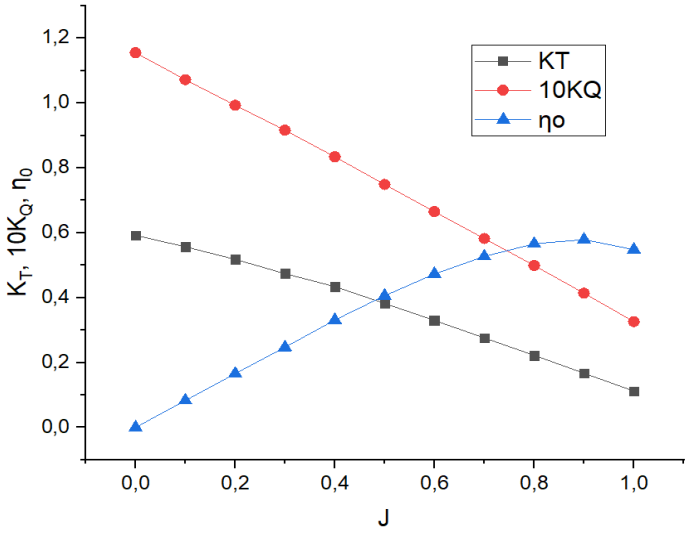

Fig. 25. Open water test diagram for Ka4-70 PBCF default

In the process of creating Figure 25, the open water test graph refers to the experimental graph from Wageningen, where the graph illustrates the values of K_T, $10K_Q$, and Efficiency (η0). Consequently, at J = 0.1, the K_T value of 0.557 decreased, reaching its lowest point at J = 1.0 with a K_T value of 0.112. Similarly, at J = 0.1, the $10K_Q$ value of 1.072 decreased, reaching its lowest point at J = 1.0 with a $10K_Q$ value of 0.326. However, in contrast, the efficiency value had the opposite trend. The efficiency was at its lowest at J = 0.1, increased at J = 0.5 with an efficiency value of 0.406, and peaked at 0.579 at J = 0.9. The visualization of pressure on the Ka4-70 propeller with Default Boss Cap Fins reinforced the results of the CFD simulation in Figure 26. In the region of the default boss cap fins, significant pressure occurred at J = 0.1, exceeding 1000 Pa; similarly, at J = 0.5, the pressure was also above 1000 Pa, but the pressure value was lower when J = 0.8, being greater than or equal to 1000 Pa. This study highlights that the Ka4-70 propeller experienced substantial pressure at low speeds, J = 0.1, up to high speeds, J = 0.8 [29].

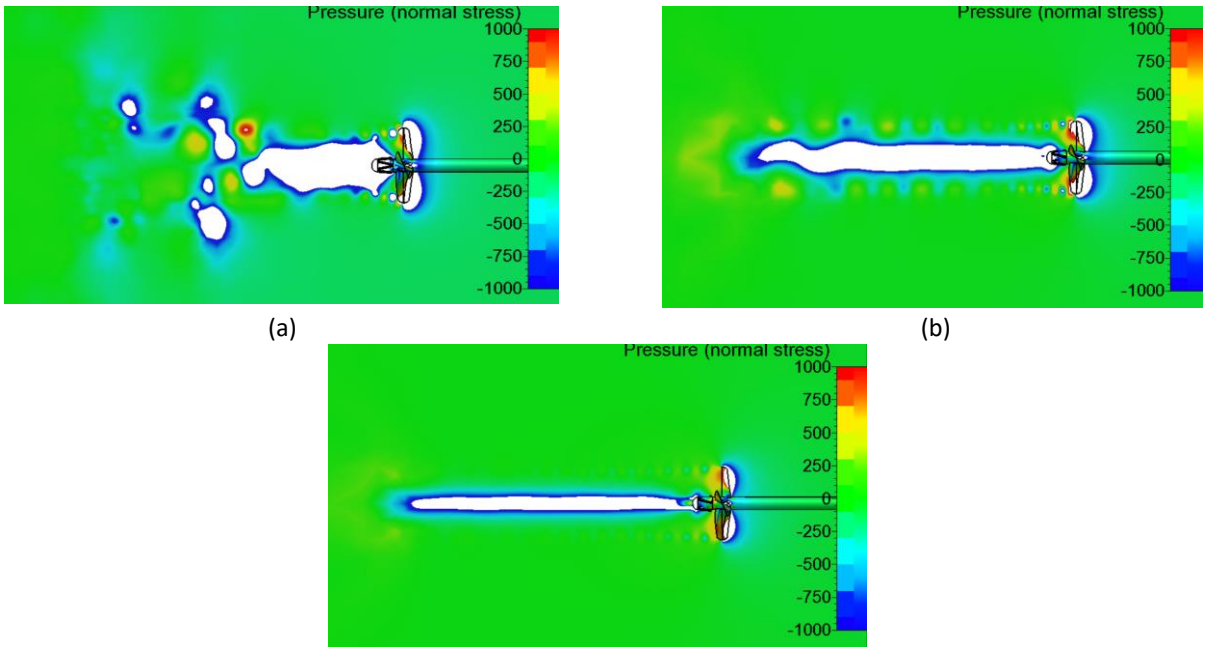

Fig. 26. Visualization of pressure on the Ka4-70 propeller with PBCF default (a) Pressure at J = 0.1 (b) Pressure at J = 0.5 (c) Pressure at J = 0.9

The visualization of the velocity of propeller Ka4-70 with BCF Default reinforced the results of the CFD simulation for pressure values, shown in Figure 27. At the boss cap fin, there was significant pressure when J = 0.1, exceeding 1000 Pa, while at J = 0.5, it remained above 1000 Pa. However, the pressure values were lower when J = 0.8, also exceeding 1000 Pa. In this study, the propeller Ka4-70 with BCF Default experienced high pressure at low speeds (J = 0.1) up to high speeds (J = 0.8), indicating a need for solutions to reduce pressure. The visualization of the velocity of propeller Ka4-70 with BCF Default reinforced the CFD simulation results for pressure values. Starting at J = 0.1, the blade section had an induced axial velocity of 3 m/s to 4 m/s, but at the boss cap of the propeller, the flow velocity ranged from 0 m/s to 4 m/s. Meanwhile, at J = 0.5, the axial induced velocity on the blade section was 3 m/s to 4 m/s, and at the boss cap of the propeller, there was flow with velocities ranging from 0 m/s to 4 m/s. When J = 0.8, the blade's induced axial velocity was 3 m/s to 4 m/s, even though there was an increase in flow velocity at the boss cap of the propeller, ranging from 0 m/s to 3 m/s. In conclusion, for propeller Ka4-70 with BCF Default, as the J value (advanced coefficient) increased, the flow velocity at the boss cap increased, while the flow velocity at the propeller blade remained the same. Therefore, solutions are needed to address the increase in flow velocity at the boss cap [31].

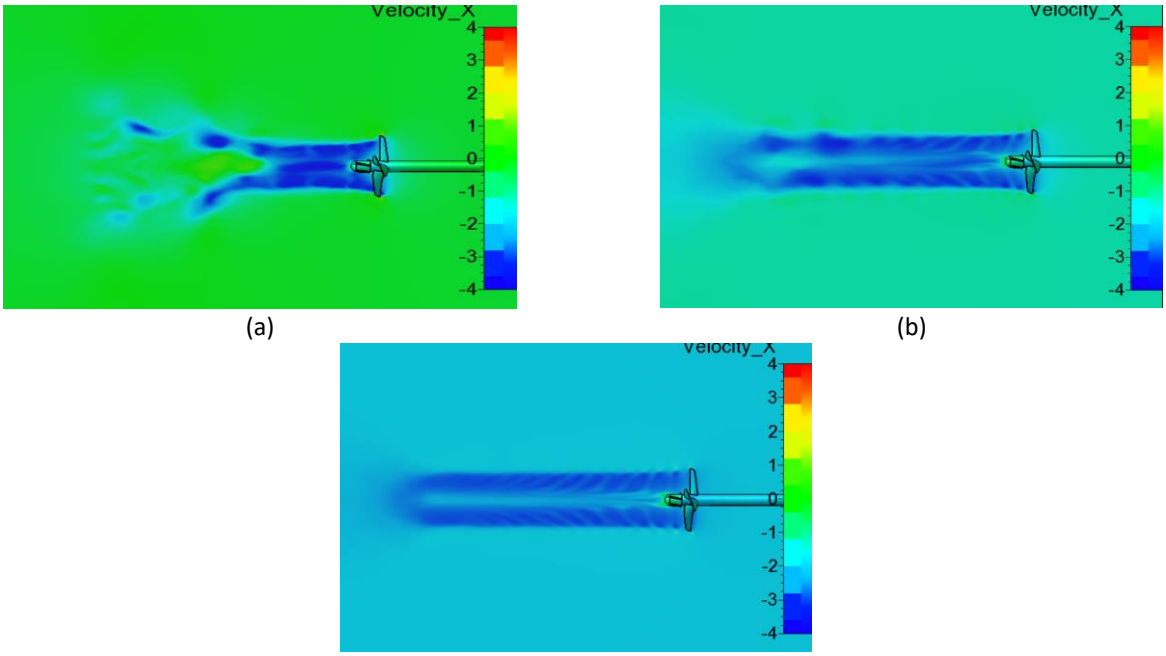

Fig. 27. Visualization of velocity on the Ka4-70 propeller with PBCF default (a) Velocity at J = 0.1 (b) Velocity at J = 0.5 (c) Velocity at J = 0.8

The results of propeller Ka4-70 with PBCF Straight calculation are shown in Figure 28.

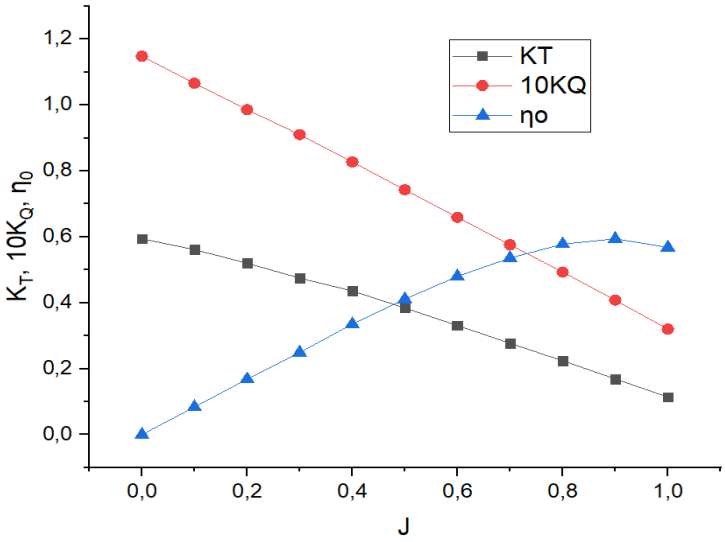

Fig. 28. Open water test diagram of Ka4-70 PBCF straight

In the process of creating Figure 28, the open water test graph refers to the experimental graph from Wageningen, where the graph illustrates the values of K_T, $10K_Q$, and Efficiency (η0). Meanwhile, at J = 0.1, the K_T value of 0.561 decreased, reaching its lowest point at J = 1.0 with a K_T value of 0.114. Similarly, at J = 0.1, the $10K_Q$ value of 1.066 decreased, reaching its lowest point at J = 1.0 with a $10K_Q$ value of 0.320. However, in contrast, the efficiency value had the opposite trend. The efficiency was at its lowest at J = 0.1, increased at J = 0.5 with an efficiency value of 0.411 [32], and peaked at 0.594 at J = 0.9 [33].

The visualization of pressure on the Ka4-70 propeller with Straight Boss Cap Fins reinforced the results of the CFD simulation in Figure 29. In the region of the straight boss cap fins, significant pressure occurred at J = 0.1, exceeding 1000 Pa; similarly, at J = 0.5, the pressure was also above 1000 Pa, but the pressure value was lower at J = 0.8, being greater than or equal to 1000 Pa. This study highlights that the Ka4-70 propeller with Straight Boss Cap Fins experienced substantial pressure at low speeds, J = 0.1, up to high speeds, J = 0.8 [34].

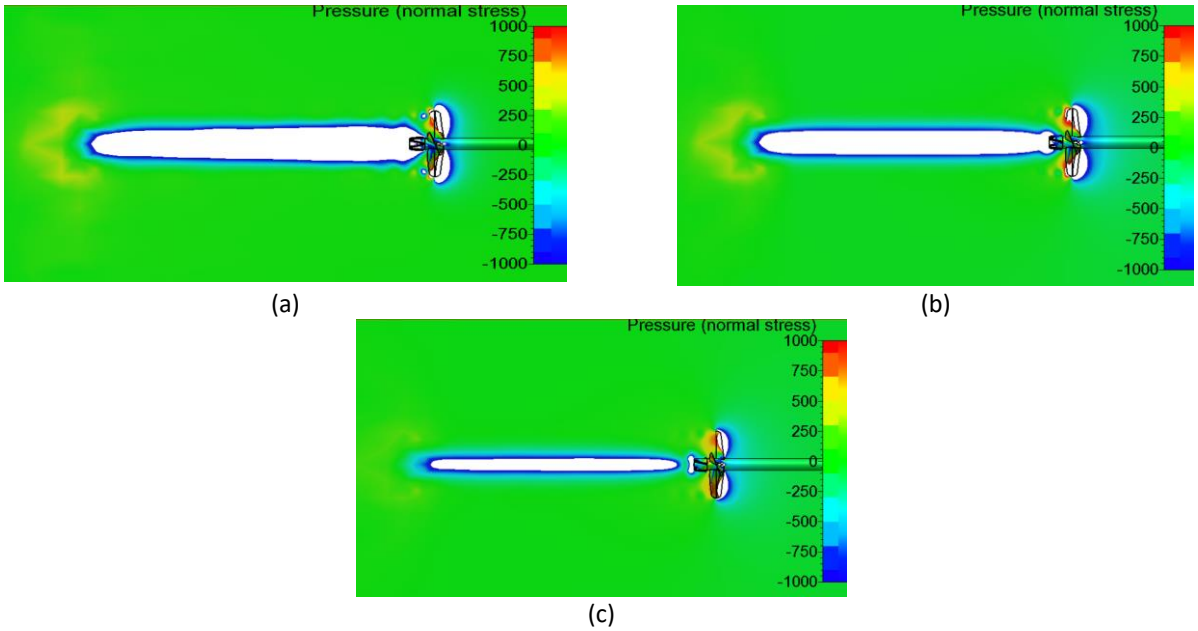

Fig. 29. Visualization of pressure on the Ka4-70 propeller with PBCF straight (a) Pressure at J = 0.1 (b) Pressure at J = 0.5 (c) Pressure at J = 0.9

The visualization of the velocity of propeller Ka4-70 with BCF Straight strengthened the results of the CFD simulation for pressure values, shown in Figure 30. At the boss cap fin, there was a significant pressure when J = 0.1, exceeding 1000 Pa, while at J = 0.5, it remained above 1000 Pa. However, the pressure values were lower when J = 0.8, also exceeding 1000 Pa. In this study, the propeller Ka4-70 with BCF Straight experienced high pressure at low speeds (J = 0.1) up to high speeds (J = 0.8), indicating a need for solutions to reduce pressure. The visualization of the velocity of propeller Ka4-70 with BCF Straight reinforced the CFD simulation results for pressure values. Starting at J = 0.1, the blade section had an induced axial velocity of 3 m/s to 4 m/s, but at the boss cap of the propeller, the flow velocity ranged from 0 m/s to 4 m/s. Meanwhile, at J = 0.5, the axial induced velocity on the blade section was 3 m/s to 4 m/s, and at the boss cap of the propeller, there was flow with velocities ranging from 0 m/s to 3 m/s. When J = 0.8, the blade's induced axial velocity was 2 m/s to 3 m/s, even though there was an increase in flow velocity at the boss cap of the propeller, ranging from 0 m/s to 2 m/s. In conclusion, for propeller Ka4-70 with BCF Straight, as the J value (advanced coefficient) increased, the flow velocity at the boss cap decreased, while the flow velocity at the propeller blade remained the same. Therefore, solutions are needed to address the increase in flow velocity at the boss cap [35].

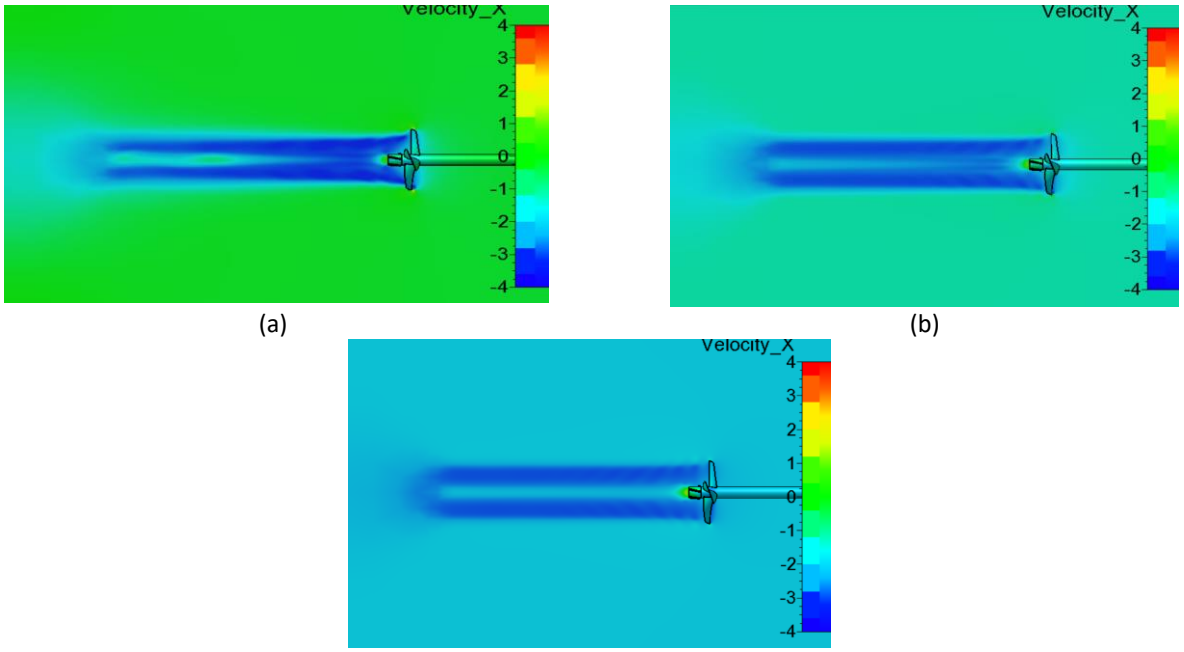

Fig. 30. Visualization of velocity on the open propeller Ka4-70 with PBCF straight (a) Velocity at J = 0.1 (b) Velocity at J = 0.5 (c) Velocity at J = 0.8

The results of propeller Ka4-70 with PBCF Convergent calculation are shown in Figure 31.

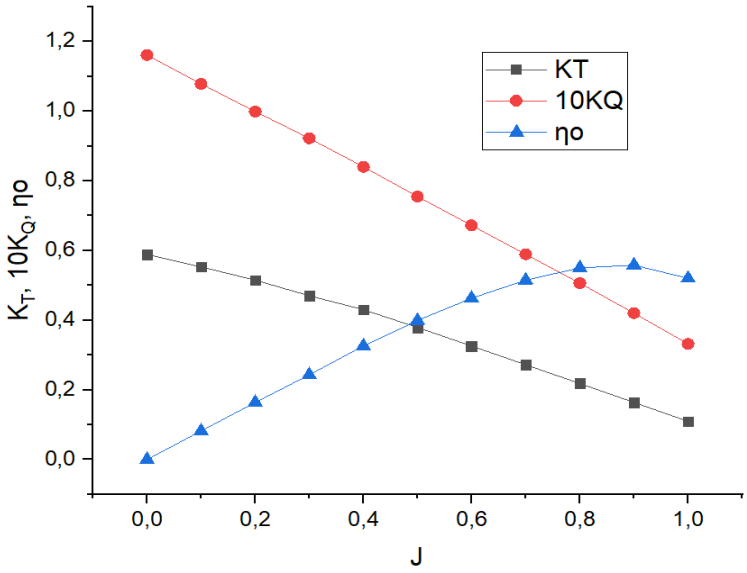

Fig. 31. Open water test diagram for Ka4-70 PBCF convergent

In the process of creating Figure 31, the open water test graph refers to the experimental graph from Wageningen, where the graph illustrates the values of K_T, $10K_Q$, and efficiency (η0). Meanwhile, at J = 0.1, the K_T value of 0.553 decreased, reaching its lowest point at J = 1.0 with a K_T value of 0.109. Similarly, at J = 0.1, the $10K_Q$ value of 1.078 decreased, reaching its lowest point at J = 1.0 with a $10K_Q$ value of 0.332. However, in contrast, the efficiency value had the opposite trend. The efficiency was at its lowest at J = 0.1, increased at J = 0.5 with an efficiency value of 0.399, and peaked at 0.558 at J = 0.9 [36]. The visualization of pressure on the Ka4-70 propeller with Convergent Boss Cap Fins reinforced the results of the CFD simulation in Figure 32. In the region of the convergent boss cap fins, significant pressure occurred at J = 0.1, exceeding 1000 Pa; similarly, at J = 0.5, the pressure was also above 1000 Pa, but the pressure value was lower at J = 0.8, ranging from 500 Pa to 1000 Pa. This study highlights that the Ka4-70 propeller with Convergent Boss Cap Fins experienced substantial pressure at low speeds, J = 0.1, up to moderate speeds, J = 0.5 [37].

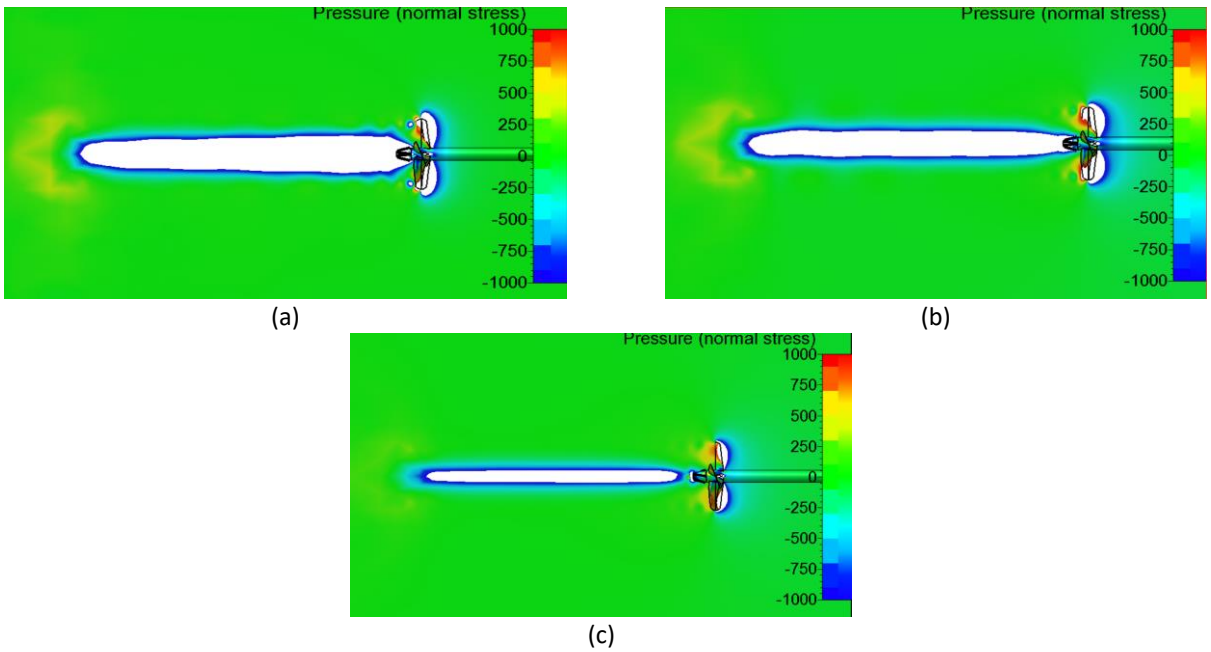

Fig. 32. Visualization of pressure on the Ka4-70 propeller with PBCF convergent (a) Pressure at J = 0.1 (b) Pressure at J = 0.5 (c) Pressure at J = 0.9

The visualization of the velocity of propeller Ka4-70 with BCF Convergent reinforced the results of the CFD simulation for pressure values, shown in Figure 33. At the boss cap fin, there was a significant pressure when J = 0.1, exceeding 1000 Pa, while at J = 0.5, it remained above 1000 Pa. However, the pressure values were lower when J = 0.8, also exceeding 1000 Pa. In this study, the propeller Ka4-70 with BCF Convergent experienced high pressure at low speeds (J = 0.1) up to moderate speeds (J = 0.5), indicating a need for solutions to reduce pressure. The visualization of the velocity of propeller Ka4-70 with BCF Convergent reinforced the CFD simulation results for pressure values. Starting at J = 0.1, the blade section had an induced axial velocity of 3 m/s to 4 m/s, but at the boss cap of the propeller, the flow velocity was 3 m/s to 4 m/s. Meanwhile, at J = 0.5, the axial induced velocity on the blade section was 3 m/s to 4 m/s, and at the boss cap of the propeller, there was flow with velocities ranging from 3 m/s to 4 m/s. When J = 0.8, the blade's induced axial velocity was 3 m/s to 4 m/s, even though there was an increase in flow velocity at the boss cap of the propeller, ranging from 1 m/s to 3 m/s. In conclusion, for Propeller Ka4-70 with BCF Convergent, as the J value (advanced coefficient) increased [38], the flow velocity at the boss cap increased, while the flow velocity at the propeller blade remained the same. Therefore, solutions are needed to address the increase in flow velocity at the boss cap.

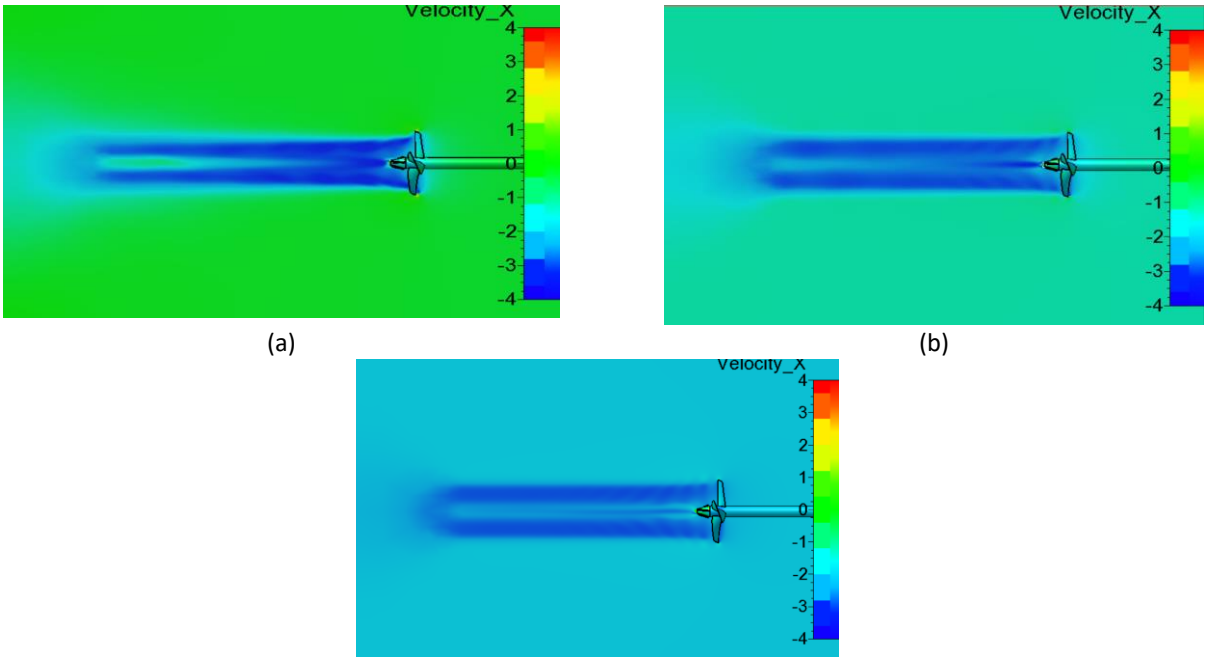

Fig. 33. Visualization of velocity on the Ka4-70 open propeller with PBCF convergent (a) Velocity at J = 0.1 (b) Velocity at J = 0.5 (c) Velocity at J = 0.8

The results of propeller Ka4-70 with PBCF Divergent calculation are shown in Figure 34.

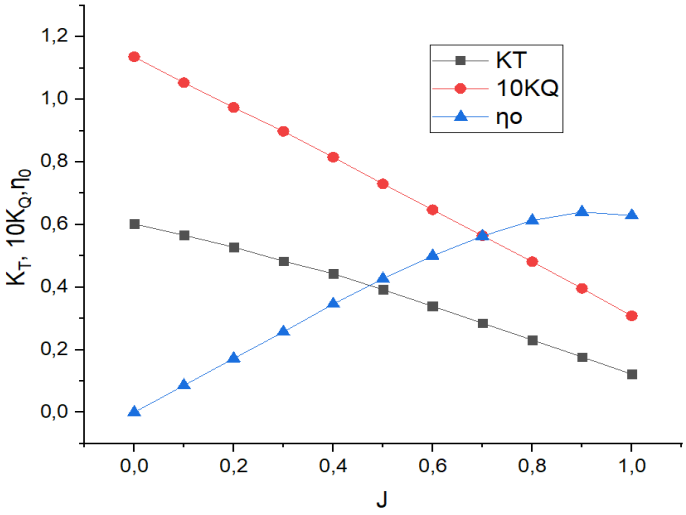

Fig. 34. Open water test diagram for Ka4-70 PBCF divergent

In the process of creating Figure 34, the open water test graph refers to the experimental graph from Wageningen, where the graph illustrates the values of K_T, $10K_Q$, and Efficiency (η0). Although, at J = 0.1, the K_T value of 0.566 decreased, reaching its lowest point at J = 1.0 with a K_T value of 0.122. Similarly, at J = 0.1, the $10K_Q$ value of 1.053 decreased [39], reaching its lowest point at J = 1.0 with a $10K_Q$ value of 0.308. However, in contrast, the efficiency value had the opposite trend. The efficiency was at its lowest at J = 0.1, increased at J = 0.5 with an efficiency value of 0.427, and peaked at 0.640 at J = 0.9 [40]. The visualization of pressure on the Ka4-70 propeller with Divergent Boss Cap Fins reinforced the results of the CFD simulation in Figure 35. In the region of the divergent boss cap fins, significant pressure occurred at J = 0.1, exceeding 1000 Pa; similarly, at J = 0.5, the pressure was also above 1000 Pa, but the pressure value was lower at J = 0.8, being greater than or equal to 1000 Pa [33]. This study highlights that the Ka4-70 propeller with Divergent Boss Cap Fins experienced substantial pressure at low speeds, J = 0.1, up to moderate speeds, J = 0.5, indicating a need for a solution to reduce the pressure [41].

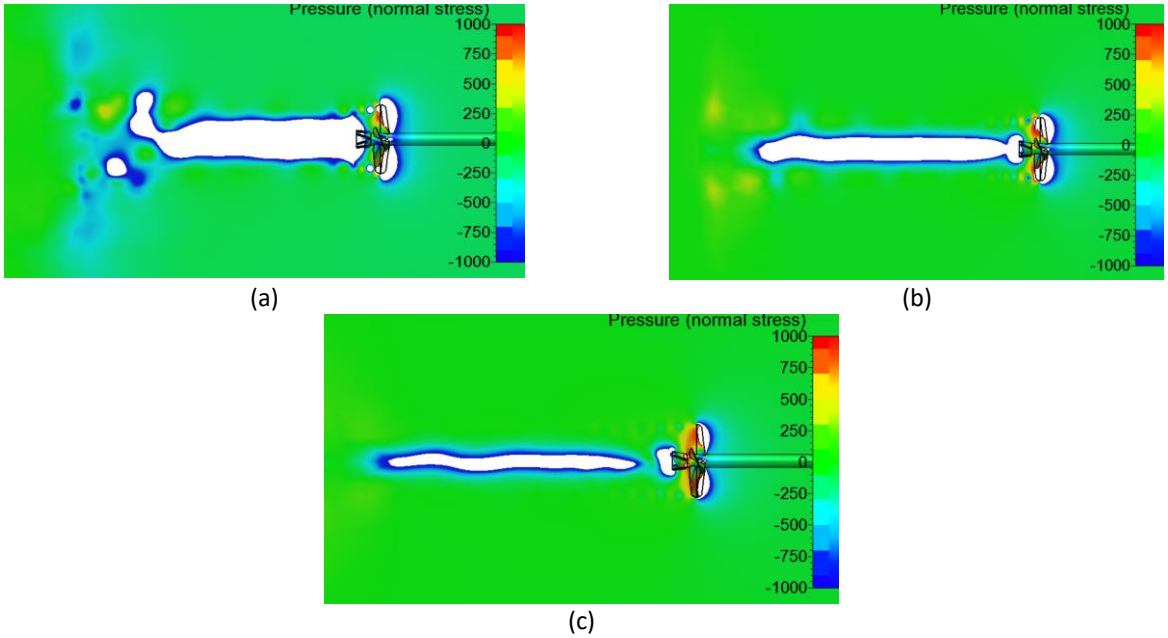

Fig. 35. Visualization of pressure on the Ka4-70 propeller with divergent boss cap fins (a) Pressure at J = 0.1 (b) Pressure at J = 0.5 (c) Pressure at J = 0.9

The visualization of the velocity of propeller Ka4-70 with BCF Divergent strengthened the results of the CFD simulation for pressure values, shown in Figure 36. At the boss cap fin, there was significant pressure when J = 0.1, exceeding 1000 Pa, while at J = 0.5, it remained above 1000 Pa. However, the pressure values were lower when J = 0.8, also exceeding 1000 Pa. In this study, the propeller Ka4-70 with BCF Divergent experienced high pressure at low speeds (J = 0.1) up to high speeds (J = 0.8), indicating a need for solutions to reduce pressure. The visualization of the velocity of propeller Ka4-70 with BCF Divergent reinforced the CFD simulation results for pressure values. Starting at J = 0.1, the blade section had an induced axial velocity of 3 m/s to 4 m/s, but at the boss cap of the propeller, the flow velocity ranged from 0 m/s to 3 m/s. Meanwhile, at J = 0.5, the axial induced velocity on the blade section was 3 m/s to 4 m/s, and at the boss cap of the propeller, there was flow with velocities ranging from 0 m/s to 3 m/s. When J = 0.8, the blade's induced axial velocity was 3 m/s to 4 m/s, even though there was an increase in flow velocity at the boss cap of the propeller, ranging from 0 m/s to 2 m/s. In conclusion, for propeller Ka4-70 with BCF Divergent, as the J value (advanced coefficient) increased, the flow velocity at the boss cap increased, while the flow velocity at the propeller blade remained the same [42]. Therefore, solutions are needed to address the increase in flow velocity at the boss cap.

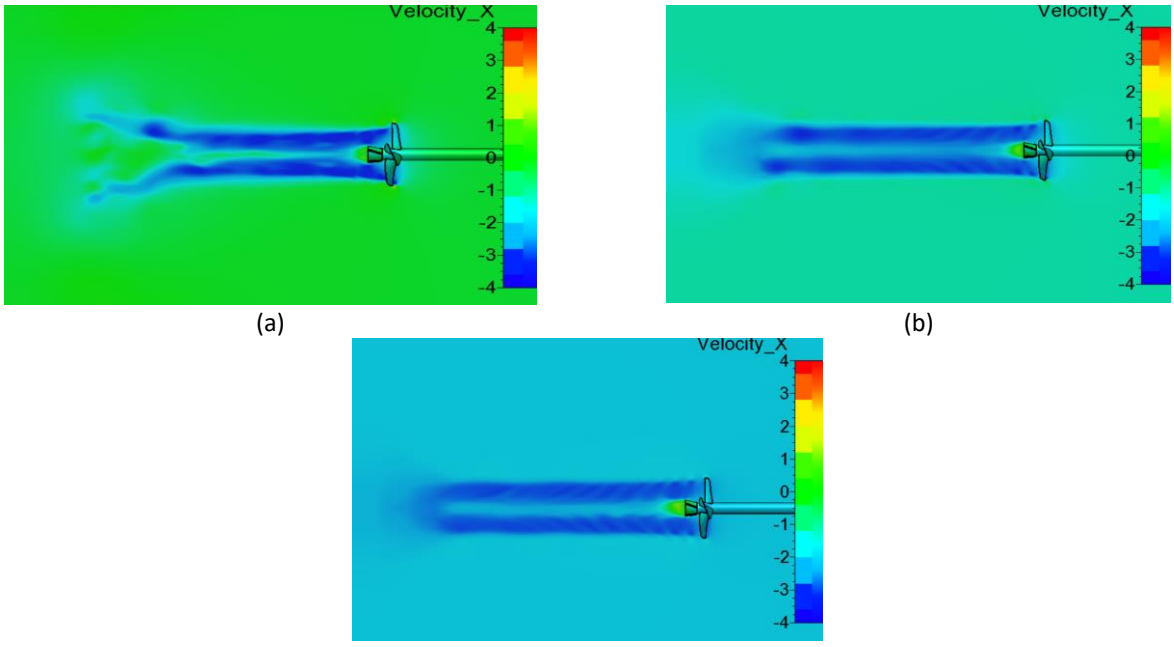

Fig. 36. Visualization of velocity on the Ka4-70 propeller with PBCF divergent (a) Velocity at J = 0.1 (b) Velocity at J = 0.5 (c) Velocity at J = 0.8

If the open propeller B4-70 and open propeller Ka4-70 were equipped with PBCF, they would experience an increase in thrust (see Figure 37). This was because the performance of the fins' functioned optimally at high J values, as indicated by high velocity values. Therefore, as the velocity increased and the pressure decreased in the boss cap area at high J values, there would be an increase in thrust due to the reduction of hub vortex [43].

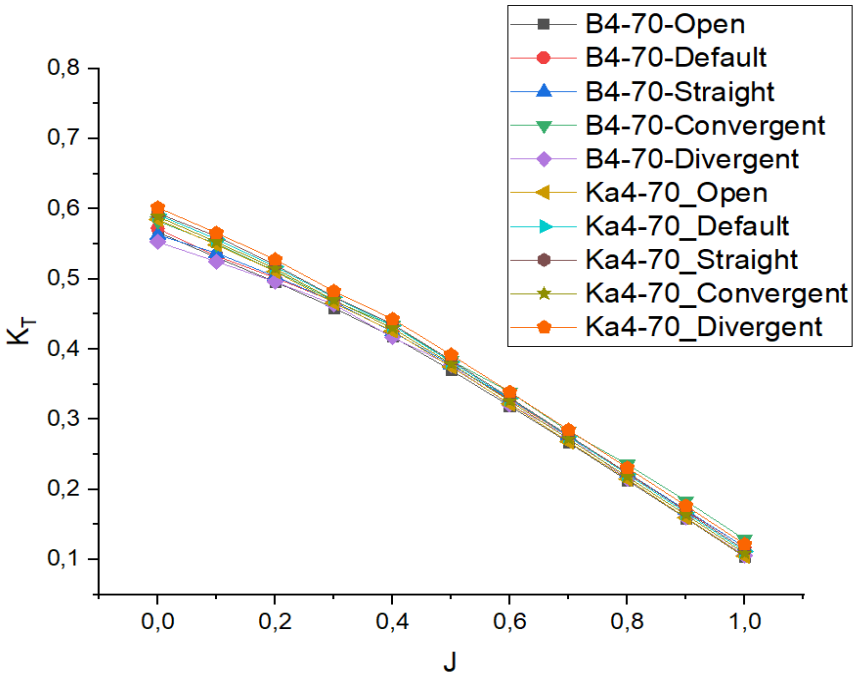

Fig. 37. K_T value graph for propeller configurations B4-70 and Ka4-70

If the open propeller B4-70 and open propeller Ka4-70 were equipped with PBCF, there would be an increase in torque accompanied by a decrease in velocity and vorticity values (see Figure 38). This was because the installation of fins on the boss cap of the propeller led to a reduction in velocity and vorticity, thereby increasing the torque requirements [44].

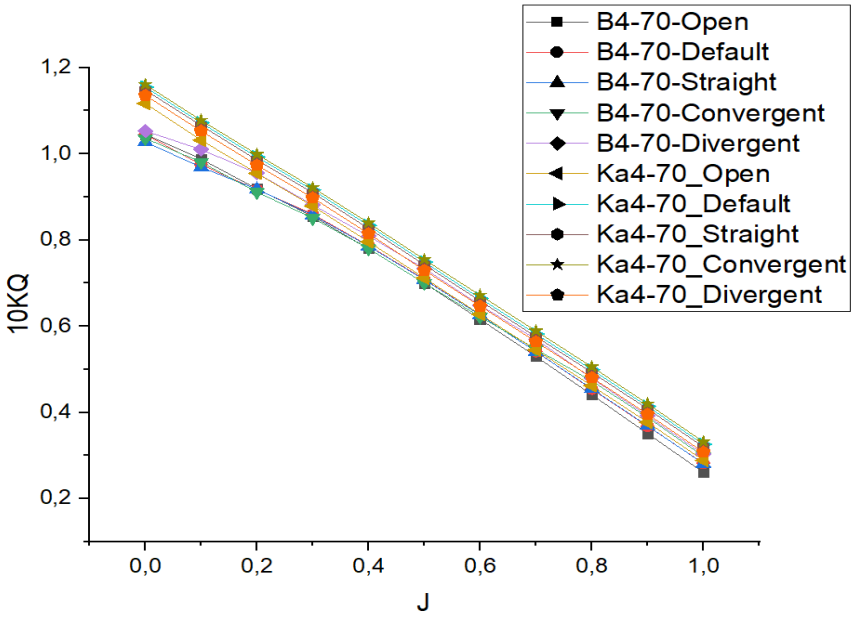

Fig. 38. $10K_Q$ value graph for propeller configurations B4-70 and Ka4-70

If the open propeller B4-70 and open propeller Ka4-70 were equipped with PBCF, there would be an increase in efficiency (η0) (see Figure 39). This was because the fins' performance was optimal at high J values, as evident from high velocity values. Therefore, as the velocity increased and the pressure decreased in the boss cap area at high J values, there would be an increase in thrust, resulting from the reduction of hub vortex, leading to enhanced efficiency [44].

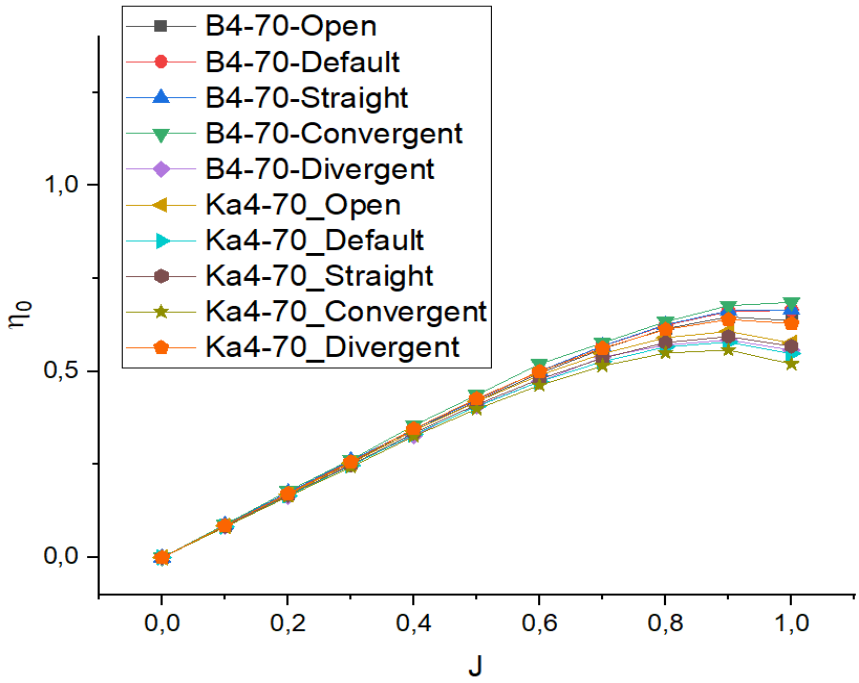

Fig. 39. η_0 value graph for propeller configurations B4-70 and Ka4-70

5. Conclusion

The design of B4-70 and Ka4-70 propellers was conducted to analyze the influence of boss cap fins on propeller efficiency. PBCF, as one of the recommended Energy-Saving Devices (ESD), was chosen due to its alignment with IMO policies for reducing greenhouse gas emissions. The research utilized the Reynolds Averaged Navier-Stokes Equation (RANSE). Based on the results and discussion, several important notes can be summarized. If the open propeller B4-70 and open propeller Ka4-70 were equipped with PBCF, there would be an increase in thrust. This was because the fins' performance was optimal at high J values, as evident from high velocity values. Therefore, as the velocity increased and the pressure decreased in the boss cap area at high J values, there would be an increase in thrust, resulting from the reduction of hub vortex. Meanwhile, when open propeller B4-70 and open propeller Ka4-70 were equipped with PBCF, there would be an increase in torque accompanied by a decrease in velocity. This was because the installation of fins on the boss cap of the propeller led to a reduction in velocity, thereby increasing torque requirements. Additionally, when open propeller B4-70 and open propeller Ka4-70 were equipped with PBCF, there would be an increase in efficiency (η0). This was due to the optimal performance of the fins at high J values, as indicated by high velocity values. As the velocity increased and the pressure decreased in the boss cap area at high J values, there would be an increase in thrust, resulting from the reduction of hub vortex. The increase in thrust was greater than the increase in torque, leading to an improvement in efficiency (η0). Specifically, for open propeller B4-70 with added PBCF, there was an increase in η0 by 3% to 5% in the range of J = 0 to J = 0.7. Similarly, for propeller Ka4-70 with added PBCF in the range of J = 0 to J = 0.7, there was an increase in η0 by 1% to 3%. This study involved comparing a propeller with added PBCF to previous studies carried out by Lim *et al.,* in 2016, Mizzi *et al.,* in 2017, Gaggero *et al.,* in 2018, and Adietya *et al.,* in 2022. The results indicated a greater efficiency improvement of 1-2% for open propellers B4-70 and Ka4-70 compared to the aforementioned studies. Based on the study, it is recommended to explore the installation of PBCF on various types and series of propellers. Additionally, it is suggested for further research to investigate the use of PBCF on different types of propellers with varying blade numbers. Notably, the use of an Energy-

Saving Device (ESD) in the form of PBCF is able to increase the efficiency of ship propeller, as reported in this paper. Consequently, these findings affirm the reliability of the overall calculations using the CFD approach.

Acknowledgements
The authors would like to express their gratitude for the assistance received from the Hydrodynamics Laboratory at the National Research and Innovation Agency. The first author extends special thanks to Diponegoro University in Semarang, Indonesia for funding the doctoral program.

References

[1] Jasper, F., and H. Shinichi. "Fourth IMO Greenhouse Gas Study 2020." *International Maritime Organisation (IMO), London, UK* (2020).
[2] DNV. 2021. "Maritime Forecast To 2050 - Energy Transition Outlook 2021." Høviky
[3] International Maritime Organization. 2021. "IMO's Work to Cut GHG Emissions from Ships
[4] International Maritime Organization 2021. "Fourth IMO GHG Study 2020 Full Report.
[5] Kawamura, Takafumi, Kazuyuki Ouchi, and Takeo Nojiri. "Model and full scale CFD analysis of propeller boss cap fins (PBCF)." *Journal of marine science and technology* 17 (2012): 469-480. https://doi.org/10.1007/s00773-012-0181-2
[6] Seo, Jeonghwa, Seung-Jae Lee, Bumwoo Han, and Shin Hyung Rhee. "Influence of design parameter variations for propeller-boss-cap-fins on hub vortex reduction." *Journal of Ship Research* 60, no. 04 (2016): 203-218. https://doi.org/10.5957/jsr.2016.60.4.203
[7] Adietya, Berlian Arswendo, I. Ketut Aria Pria Utama, and Wasis Dwi Aryawan. "CFD Analysis into the Effect of using Propeller Boss Cap Fins (PBCF) on Open and Ducted Propellers, Case Study with Propeller B-Series and Kaplan-Series." *CFD Letters* 14, no. 4 (2022): 32-42. https://doi.org/10.37934/cfdl.14.4.3242
[8] Ridwan, M., B. A. Adietya, and D. Chrismianto. "Stability analysis of trawls type traditional fishing boat with modification of eco-friendly fishing-gear on the north coast of Central Java." In *IOP Conference Series: Materials Science and Engineering*, vol. 403, no. 1, p. 012052. IOP Publishing, 2018. https://doi.org/10.1088/1757-899X/403/1/012052
[9] Kiryanto, Mohammad Ridwan, Berlian Arswendo Adietya, Deddy Chrismianto, and Sri Hartanto Aji Sasongko. "Stability and total resistance analysis of catamaran fishing boat for Java North Sea area with hullform model and fishing gear variation." *International Journal of Mechanical Engineering and Technology (IJMET) Vol* 10, no. 01 (2019): 1291-1302.
[10] Chrismianto, Deddy, Ahmad Fauzan Zakki, Berlian Arswendo, and Insanu Abdilla Cendikia Abar. "Comparison of Propeller Type B-Series and Au-Outline Gawn Series for Improving on Submarine Propulsion Performance using CFD." *International Journal of Advanced Research in Engineering and Technology* 10, no. 2 (2019). https://doi.org/10.34218/IJARET.10.2.2019.061
[11] Adietya, Berlian Arswendo, Aulia Windyandari, and Ahmad Fauzan Zakki. "The Study on Stability and Seakeeping Characteristics of the Glass Bottom Boat Trimaran in Karimunjawa Island." In *IOP Conference Series: Earth and Environmental Science*, vol. 135, no. 1, p. 012007. IOP Publishing, 2018. https://doi.org/10.1088/1755-1315/135/1/012007
[12] Ariana, I. Made, Riyan Bagus Prihandanu, Dhimas Widhi Handani, and A. A. B. Dinariyana. "Investigation of the Effects of the Pre-Duct in a Ship on Propeller–Hull Interactions Using the CFD Method." *CFD Letters* 15, no. 4 (2023): 17-30. https://doi.org/10.37934/cfdl.15.4.1730
[13] International Maritime Organization. 2009. *Guidelines for Voluntary Use of the Ship Energy Efficiency Operational Indicator*. Vol. MEPC.1/Circ. London: International Maritime Organization – Part b
[14] Mewis, Friedrich. "A novel power-saving device for full-form vessels." In *First International Symposium on Marine Propulsors, SMP*, vol. 9. 2009.
[15] Celik, Ishmail B., Urmila Ghia, Patrick J. Roache, and Christopher J. Freitas. "Procedure for estimation and reporting of uncertainty due to discretization in CFD applications." *Journal of fluids Engineering-Transactions of the ASME* 130, no. 7 (2008). https://doi.org/10.1115/1.2960953
[16] Darsono, Febri Budi, Rahmad Doni Widodo, and Akhmad Nurdin. "Analysis Of the Effect of Flow Rate and Speed on Four Blade Tubular Water Bulb-Turbine Efficiency Using Numerical Flow Simulation." *Journal of Advanced Research in Fluid Mechanics and Thermal Sciences* 90, no. 2 (2021): 1-8. https://doi.org/10.37934/arfmts.90.2.18
[17] Niknahad, Ali. "Numerical study and comparison of turbulent parameters of simple, triangular, and circular vortex generators equipped airfoil model." *Journal of Advanced Research in Numerical Heat Transfer* 8, no. 1 (2022): 1-18.

[18] Wallin, Stefan. *Engineering turbulence modelling for CFD with focus on explicit algebraic Reynolds stress models*. Stockholm, Sweden: Royal Institute of Technology, Department of Mechanics, 2000.
[19] Xing, L. H., G. B. Huang, and Min Yan. "Numerical Simulation of 3D Density Flow by an Improved EASM Model." *Procedia Environmental Sciences* 10 (2011): 753-758. https://doi.org/10.1016/j.proenv.2011.09.122
[20] Matsuda, Satoshi, and Tokihiro Katsui. "Hydrodynamic Forces and Wake Distribution of Various Ship Shapes Calculated Using a Reynolds Stress Model." *Journal of Marine Science and Engineering* 10, no. 6 (2022): 777. https://doi.org/10.3390/jmse10060777
[21] Carlton, John. 2019. "Thrust Augmentation Devices." In *Marine Propellers and Propulsion*, 367–78. Elsevier. https://doi.org/10.1016/B978-0-08-100366-4.00013-4
[22] Mizzi, Kurt, Yigit Kemal Demirel, Charlotte Banks, Osman Turan, Panagiotis Kaklis, and Mehmet Atlar. "Design optimisation of Propeller Boss Cap Fins for enhanced propeller performance." *Applied Ocean Research* 62 (2017): 210-222. https://doi.org/10.1016/j.apor.2016.12.006
[23] Bahatmaka, Aldias, Aditya Rio Prabowo, and Dong-Joon Kim. "Effect of Nozzle Performance on the Ducted Propeller: A Benchmark-Simulation Study using OpenFOAM." *Transportation Research Procedia* 55 (2021): 645-652. https://doi.org/10.1016/j.trpro.2021.07.031
[24] Gatski, Thomas B., and Charles G. Speziale. "On explicit algebraic stress models for complex turbulent flows." *Journal of fluid Mechanics* 254 (1993): 59-78. https://doi.org/10.1017/S0022112093002034
[25] Gao, Qiuxin, Wei Jin, and Dracos Vassalos. "The calculations of propeller induced velocity by RANS and momentum theory." *Journal of Marine Science and Application* 11, no. 2 (2012): 164-168. https://doi.org/10.1007/s11804-012-1118-1
[26] Anderson, John David, and John Wendt. 1995. *Computational Fluid Dynamics*. Vol. 206. Berlin: Springer
[27] Hsin, Ching-Yeh, Bo-Hong Lin, and Chung-Ching Lin. "The optimum design of a propeller energy-saving device by computational fluid dynamics." In *Computational Fluid Dynamics 2008*, pp. 655-660. Springer Berlin Heidelberg, 2009. https://doi.org/10.1007/978-3-642-01273-0_87
[28] Gaggero, Stefano, Juan Gonzalez-Adalid, and Mariano Perez Sobrino. "Design and analysis of a new generation of CLT propellers." *Applied Ocean Research* 59 (2016): 424-450. https://doi.org/10.1016/j.apor.2016.06.014
[29] Ghassemi, Hassan, Amin Mardan, and Abdollah Ardeshir. "Numerical analysis of hub effect on hydrodynamic performance of propellers with inclusion of PBCF to equalize the induced velocity." *Polish Maritime Research* 19, no. 2 (2012): 17-24. https://doi.org/10.2478/v10012-012-0010-x
[30] Hansen, Hans Richard, Tom Dinham-Peren, and Takeo Nojiri. "Model and full scale evaluation of a 'propeller boss cap fins' device fitted to an Aframax tanker." In *Second International Symposium on Marine Propulsors*. 2011.
[31] Gaggero, Stefano, Diego Villa, Giorgio Tani, Michele Viviani, and Daniele Bertetta. "Design of ducted propeller nozzles through a RANSE-based optimization approach." *Ocean Engineering* 145 (2017): 444-463. https://doi.org/10.1016/j.oceaneng.2017.09.037
[32] Lim, Sang-Seop, Tae-Won Kim, Dong-Myung Lee, Chung-Gil Kang, and Soo-Young Kim. "Parametric study of propeller boss cap fins for container ships." *International Journal of Naval Architecture and Ocean Engineering* 6, no. 2 (2014): 187-205. https://doi.org/10.2478/IJNAOE-2013-0172
[33] Nojiri, Takeo, Norio Ishii, and Hisashi Kai. "Energy saving technology of PBCF (Propeller Boss Cap Fins) and its evolution." *マリンエンジニアリング* 46, no. 3 (2011): 350-358. https://doi.org/10.5988/jime.46.350
[34] Eom, Myeong-Jin, Yoon-Ho Jang, and Kwang-Jun Paik. "A study on the propeller open water performance due to immersion depth and regular wave." *Ocean Engineering* 219 (2021): 108265. https://doi.org/10.1016/j.oceaneng.2020.108265
[35] Atlar, M. "An investigation into effective boss cap designs to eliminate propeller hub vortex cavitation." *Proceedings of PRADS'98* (1998): 757-769. https://doi.org/10.1016/S0928-2009(98)80220-5
[36] Seo, Jeonghwa, Seung-Jae Lee, Bumwoo Han, and Shin Hyung Rhee. "Influence of design parameter variations for propeller-boss-cap-fins on hub vortex reduction." *Journal of Ship Research* 60, no. 04 (2016): 203-218. https://doi.org/10.5957/jsr.2016.60.4.203
[37] Adietya, Berlian Arswendo, I Ketut Aria Pria Utama, Wasis Dwi Aryawan, Mochammad Nasir, Nurcholis, Mahendra Indiaryanto, Nurwidhi Asrowibowo, Rizqi Dian Permana, and Nurhadi. 2023. "Numerical and Experimental Investigations into the Characteristics of Wageningen B4-70 Series of Propeller with Boss Cap Fins." *CFD Letters* 15, no. 10 (2023): 152–169. https://doi.org/10.37934/cfdl.15.10.152169
[38] Adietya, Berlian Arswendo, I. Ketut Aria Pria Utama, Wasis Dwi Aryawan, Dwi Wahyudi, Anis Kurniati Arifah, Baharuddin Ali, and Bashofi Cahyo Buwono. "Characteristics Investigations of Ducted Ka4-70 Series Propeller with Boss Cap Fins Using Numerical and Experimental Method." *CFD Letters* 16, no. 2 (2024): 24-41. https://doi.org/10.37934/cfdl.16.2.2441

[39] Trimulyono, Andi, A. B. Jatmiko, I. P. Mulyatno, and H. Yudo. "The effect of propeller cap angle and fin size of PBCF on propeller performance." In *IOP Conference Series: Earth and Environmental Science*, vol. 972, no. 1, p. 012045. IOP Publishing, 2022. https://doi.org/10.1088/1755-1315/972/1/012045

[40] Trimulyono, A., I. P. Mulyatno, and A. F. Rachmat. "The Effect of Mewis Duct Energy Saving Device to Propeller Performance." In *IOP Conference Series: Earth and Environmental Science*, vol. 1098, no. 1, p. 012076. IOP Publishing, 2022. https://doi.org/10.1088/1755-1315/1098/1/012076

[41] Adietya, Berlian Arswendo, Husein Syahab, Mochammad Nasir, Wasis Dwi Aryawan, and I Ketut Aria Pria Utama. 2023. "Numerical Analysis into the Improvement Performance of Ducted Propeller by Using Fins: Case Studies on Types B4-70 and Ka4-70." *CFD Letters (Accepted for Publication)*

[42] Adietya, B. A., W. D. Aryawan, and I. K. A. P. Utama. "A study into the effect of tip clearance on the performance of b-series and kaplan-series ducted propellers." In *IOP Conference Series: Earth and Environmental Science*, vol. 1166, no. 1, p. 012038. IOP Publishing, 2023. https://doi.org/10.1088/1755-1315/1166/1/012038

[43] Stern, Fred. 2014. *Mechanics of Fluids and Transport Processes*. 57:020. Iowa City: University of Iowa.

[44] Molland, Anthony F., Stephen R. Turnock, and Dominic A. Hudson. *Ship resistance and propulsion*. Cambridge university press, 2017. https://doi.org/10.1017/9781316494196